

NGU Report 2000.081

LA-HR-ICP-MS analysis of quartz and
principles governing the distribution and
speciation of structural impurities in
igneous quartz

REPORT

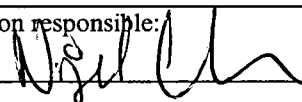
Report no.: 2000.081		ISSN 0800-3416	Grading: Open
Title: LA-HR-ICP-MS analysis of quartz and principles governing the distribution and speciation of structural impurities in igneous quartz			
Authors: Rune B. Larsen, Belinda Flem, Siv Dundas, Yann Lahaye and Joakim Mansfeld		Client: NGU, North Cape Minerals	
County: Aust Agder		Commune:	
Map-sheet name (M=1:250.000)		Map-sheet no. and -name (M=1:50.000)	
Deposit name and grid-reference:		Number of pages: 43	Price (NOK):
		Map enclosures:	
Fieldwork carried out: 1996-1998	Date of report: 12 July 2000	Project no.: 2728.00	Person responsible: 
<p>Summary: Laser Ablation High Resolution Inductively Coupled Plasma Mass Spectrometry (LA-HR-ICP-MS) of quartz is now fully operational at NGU and may be applied as an exploration method after new high-purity quartz deposits. The analytical method may also be important in characterising which parts of an already existing mining operation that contain the best qualities of quartz. In mapping the quality of quartz throughout an existing mine, it may aid the producer in optimising the potential of the quartz raw material and overall may be an important guide in the day-to-day operation of the quarry.</p> <p>Compared with conventional methods for the analysis of quartz, the analytical method developed at NGU is faster and cheaper, and minimizes the risk of contamination of the sample.</p> <p>Although the analytical method is applicable as it stands, it would in the long term be desirable to improve the precision of Al and Li. Recent improvements and analysis of well-characterized samples imply that this problem is near its solution.</p> <p>Analysis of Ca may be possible after the manufacture of better standards and B may be quantified if pre-ablation of the sample surface is applied and if the analyses of Li₂B₄O₇ tablets remain discontinued at NGU with the LA-HR-ICP-MS instrument</p> <p>Studies of granite pegmatite quartz in Evje-Iveland and Froland imply that systematic XRF-analysis of selected minerals in granite pegmatites may aid in defining areas where the prospecting after high-purity quartz is most beneficial. In many pegmatite fields, this has already been accomplished so that laser ablation of quartz may proceed right away. Studies of the concentration of Al, Be, Mg, K, Ti, Cr, Mn, Fe, Ge, Rb, Sr, Ba, Pb, Th, and U in quartz from Evje-Iveland and Froland unequivocally demonstrate that granite pegmatite quartz in Froland is more pure than Evje-Iveland quartz. The main benefit of the Froland quartz is the low contents of Al, Li and Na. However, the concentration of Ti remains quite high although, on the average, it is lower than Evje-Iveland quartz. The trace element distribution in quartz follows the petrogenetic evolution of K-feldspar, which is governed by processes of igneous differentiation in the pegmatite melts. Accordingly, speciation and quantity of structural admixtures in quartz is also governed by the igneous evolution of the pegmatite forming melt. Following this principle, the purity, i.e. the quality of quartz, in the Evje-Iveland and Froland pegmatite fields is proportional to the degree of differentiation of the pegmatite forming liquids. In other words, the concentration of structural elements incorporated in the quartz crystal structure becomes progressively lower as igneous differentiation proceeds from primitive to more evolved granite pegmatite melts. In Evje-Iveland, the spatial distribution of the major structural impurities (Al, Li, Na, Ti) decreases in a westerly direction. This trend coincides with studies of K-feldspar (Larsen <i>in prep.</i>) that implies that the most primitive pegmatites occur in North and towards East of the Evje-Iveland pegmatite field.</p>			
Keywords:	Industrial minerals	Quartz	
Trace elements	High-purity quartz	LA-HR-ICP-MS	
Granite Pegmatites			

TABLE OF CONTENTS

1. INTRODUCTION	4
2. BACKGROUND	5
3. GEOLOGY OF QUARTZ	6
4. ANALYTICAL STRATEGY	9
4.1 Public summary of analytical approach	10
4.2 Experimental approach used at NGU	12
4.3 Experimental approach used at VIEPS	17
5. COMPOSITION AND GEOLOGICAL SETTING OF PEGMATITE QUARTZ	20
5.1 Geological setting	20
5.2 Trace element distribution in quartz	23
6. DISCUSSION	28
6.1 Analytical strategies	28
6.2 Composition of quartz compared to granite pegmatite evolution	29
6.3 Exploration strategies	31
7. CONCLUSIONS	33
7.1 Industrial application of results	33
7.2 Structural impurities in quartz	33
7.3 Analytical strategies	34
8. RECOMMENDATIONS	35
9. ACKNOWLEDGEMENT	35
10. REFERENCES	36
11. APPENDIX	40

1. INTRODUCTION

The present communication comprises the final report in the project "High-purity quartz in Norway", a project that was launched in 1997 and now, after nearly four years of studies is finally concluding with a novel analytical method for *in situ* chemical analysis of quartz and a preliminary model explaining the distribution and speciation of trace elements in igneous quartz. Together, this knowledge may be of profound help in the prospecting after high-purity quartz deposit in igneous, metamorphic and sedimentary terrains. Furthermore, it may provide us with a more thorough understanding of the principles that govern concentration and speciation of foreign elements incorporated in quartz during processes of igneous differentiation.

In summarising the scope of the project, one may as well cite the original project proposal from 1997 that boil down the primary goal to the following four points:

- 1) To study and characterise physical and chemical parameters favouring the genesis of high-purity quartz in granite pegmatites
- 2) To evaluate the resources of high-purity pegmatite quartz in South-Norway
- 3) Based on (1) to develop a field methods that succeed in distinguishing between high- and low purity quartz in a given area
- 4) Also based on (1) To develop a low cost laboratory procedure that can be used to evaluate the potential of a pegmatite to comprise high purity quartz

The original area was defined as all of Norway, or more precisely the Tysfjord-Innhavet area, Pasvik and Telemark/Setesdalen. In the end, however, it was decided only to focus on southern Norway (Fig 1) because the pegmatite fields in this area have been studied in greater detail in terms of geometry and mineralogy and because it was possible to find an industrial collaboration partner committed to this area.

In various versions of the project proposal that circulated after the original cited above, granitoid-quartz was also included in the study. However, it was soon realized that analytical obstacles consumed the time allotted to the study of granitoid rocks. The study of quartz in granitic rocks (diorites, granodiorites, monzonites, granites etc.) is very interesting from an

academic point of view. However, from an industrial perspective, numerous analyses invalidate granite-quartz as a feasible industrial resource because the concentrations of structural impurities in quartz from these lithologies are far too high (e.g. Dennen et al., 1970).



Figure 1: Location of the studied area.

With this report it may be forwarded that the goals stated in the four points above are fulfilled. We now understand some of the processes that influence the incorporation of impurities in quartz and know how to apply this knowledge in focused prospecting after high-purity quartz deposits. Furthermore, we have developed a laser ablation method that is rapid, cheap and requires a minimum of sample preparation which can be applied in regional exploration after high purity quartz occurrences and in detailed element mapping of operating quartz-quarries.

2. BACKGROUND

High-purity quartz is common quartz that is characterized by exceptionally low concentrations of elements other than silicon and oxygen. Untreated, naturally occurring quartz with less than 50 ppm of impurities qualifies as high-purity quartz; however, quartz with as much as 500 ppm total impurities may suffice if industrially feasible dressing techniques succeed in lowering the impurity level to less than 50 ppm. Given these

specifications, prices in excess of 1000 US\$ /ton may be obtained in a market which, according to a 1992 Roskill report "*The Economics of Quartz*", is stipulated to increase by 5-8% per annum. The *USGS Minerals Information* also forecasts solid growth in the demand for high-purity quartz, - not least as a result of continued expansion in the production of silicon oxide wafers for semi-conductor technology. High-purity quartz is largely used to manufacture *silica glass*, which is formed by melting processed crystalline quartz at temperatures between 1750 and 2000 °C. The final product contains > 99.995% SiO₂ and, because of its outstanding chemical and physical properties, silica glass is the only single-component glass that has wide commercial applications (Fanderlik 1991). The most important properties of silica glass are resistance to extreme fluctuations in temperature, chemical durability in acidic environments and its ability of transmitting light from near ultraviolet to infrared parts of the spectrum. Therefore, silica glass has found wide applications in the metallurgical, chemical and optical industries, as well as in communication technology for the manufacture of optical wave-guides. An exciting application is as a raw material in the development of high-performance solar panels for energy production.

3. GEOLOGY OF QUARTZ

The following outline is primarily extracted from work by Dennen (1964, 1967), Dennen et al. (1970), Lehmann & Bambauer (1973), Fanderlik (1991), Jung (1992), Perny et al. (1992), Deer et al. (1997), and Watt et al. (1997). Other sources are cited in the text. In evaluating the quality of quartz, distinguishing between structural impurities, solid and liquid inclusions (Fig 2), is imperative. Solid and liquid inclusions are evaluated only briefly at the end of this section because, to a large extent, they are removed during the processing of quartz unless they are small and/or very abundant. Structural impurity elements, on the contrary, can only be partially removed by time-consuming and expensive dressing techniques. Therefore, it is the concentration of these elements that ultimately distinguishes high-purity quartz deposits from inferior quality occurrences.

The speciation and character of impurities in quartz are non-obvious features that complicate prospecting for high-purity quartz resources. For example, quartz, which at first glance appears clear and inclusion-free, may contain thousands of ppm of structural impurities. On the contrary, dark smoky quartz with many solid and liquid inclusions may provide an excellent raw material for certain applications if the inclusions can be removed

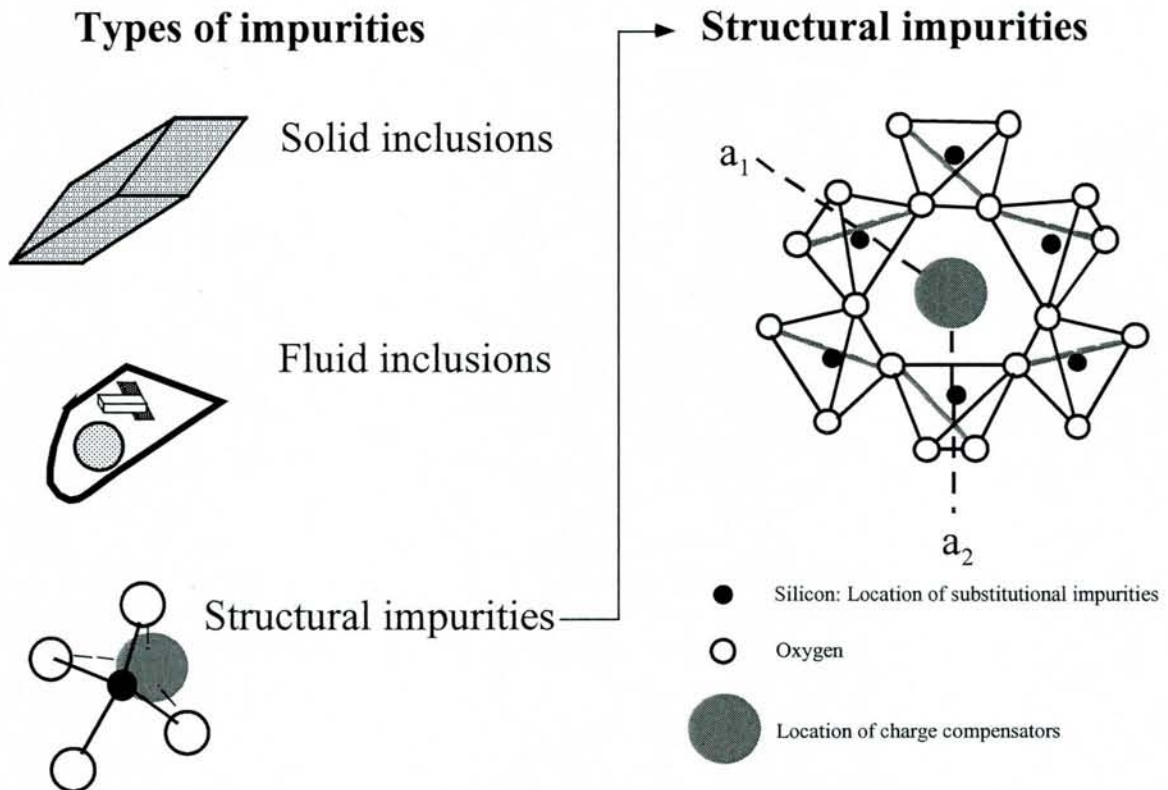


Figure 2: This figure illustrates the types of impurities that are common in quartz. The left part of the figure illustrates different types of impurities, i.e. solid inclusions, fluid inclusions and structural impurities. The right hand figure shows types of structural impurities. Locations of structural impurities (figure to the right) are shown for β -quartz, which is the most common type of quartz at the Earth's surface and is the only type of quartz found in the Evje-Iveland area. Also to the right, the atomic configurations of silicon and oxygen are viewed in a section perpendicular to the crystallographic c -axis. a_1 and a_2 denotes crystallographic axes.

through affordable industrial dressing methods. This is because the smoky colour of quartz is caused by low levels of ionising radiation induced by the decay of radioactive elements in neighbouring minerals (e.g. ^{40}K in alkali feldspar), whereas the quartz itself may contain only a few ppm of structurally bound impurities that, however, are confined to colour centres in the atomic lattice, hence inducing the smoky colour. Other colour variations may indeed be signs of abundant structural impurities, such as in amethyst, for example, that owes its colour to structurally bound Fe (e.g. Aines & Rossmann 1986, Cohen 1985, Hassan & Cohen 1974); and rose quartz colours which, according to some studies, are due to high concentrations of structurally bound Fe and Ti (e.g. Hassan & Cohen 1974, Cohen & Makar 1984, 1985), Al-P substitutions (Maschmeyer & Lehmann 1983) or, according to recent studies, are caused by inclusions of sub-microscopic dumortierite $[\text{Al}_7(\text{BO}_3)(\text{SiO}_4)\text{O}_3]$ fibres (Julia Goreva, unpublished).

Quartz has an exceptionally strong atomic configuration of Si-O bonds that allows only a minimum of other elements into its structure. However, minute amounts of substitutional and

interstitial impurities may be incorporated into the atomic lattice and these elements are classified as structural impurities. Elements that are most commonly identified as structural impurities encompass Al, B, Ca, Cr, Cu, Fe, Ge, H, K, Li, Mg, Mn, Na, P, Pb, Rb, Ti and U. Not all studies agree with this list of elements. Jung (1992) suggested that only Al, B, Ge, Fe, H, K, Li, Na, P and Ti may be regarded as true structural impurities, whereas Ca, Cr, Cu, Mg, Mn, Pb, Rb and U are the results of contamination by microscopic solid and liquid inclusions which were not entirely removed before analysis. Another reason for this apparent controversy may be the fact that certain elements, e.g. the alkali metals, tend to form minute atomic clusters adsorbed at specific growth directions i.e. the 0001 surface (Brouard et al. 1995). Forming adsorbed clusters, they hardly classify as conventional structural impurities. However, being strictly confined to one growth direction, the incorporation of atomic clusters is dependent on the physics, and hence on the atomic lattice properties, of specific crystallographic orientations. As they are not so strongly arrested in the quartz structure as compared with conventional structural impurities, atomic clusters may be more exposed to acid leach and, therefore, may be partially or fully removed during processing of the quartz raw material.

Substitutional impurities compete with Si^{4+} in the Si-O tetrahedron composing the quartz lattice (Fig. 2), whereas interstitial impurities mostly include small monovalent ions that fit into structural channels running parallel to the c-axis and function as charge compensators balancing substitutional impurities (Fig 2). Al^{3+} , for example, is a common substitutional impurity whereas Li^+ or Na^+ , in the structural channels, balances the missing positive charge. Next to aluminium, Ti, Fe and Ge are common substitutions for Si whereas H, Li, Na and K (e.g. Watt et al. 1997) are common charge compensators. However, H is rare in magmatic quartz, whereas it dominates over the other common charge compensators in quartz that formed from dilute aqueous solutions, e.g. in alpine-type quartz veins. This latter type of quartz, occasionally featuring lamellar growth structures, is also known for highly asymmetric distributions of structural impurities giving rise to sectoral or concentric zonation patterns brought about by selective accumulation along specific growth orientation of certain elements (e.g. Paquette & Reeder 1995). In single crystals of some lamellar quartz, for example, the concentration of Al may experience an abrupt increase from 20 ppm in one growth sector to 620 ppm in a neighbouring growth sector of the same crystal.

Highly uneven distributions of impurities are limited to lamellar hydrothermal vein quartz, whereas structural impurities in igneous and metamorphic quartz are more evenly distributed throughout individual crystals.

It is challenging to try to forecast the specific geological environment that most favours the genesis of high-purity quartz. Traditionally, high-purity quartz is recovered from quartz veins and granite pegmatites. Brazil and Madagascar, in particular, were leading producers of vein-type high-purity quartz whereas, today, the Spruce Pine pegmatite district in North America is almost the solitary world supplier. Recently, the production of high-purity quartz from Drag, North Norway, recommenced after a near 10-year period of inactivity and quartz production from the Drag granite pegmatites has now been in operation for more than 3 years.

In most minerals, there is a crude positive correlation between crystallization temperature and the concentration of structural impurities, and this relationship also applies to structural impurities in quartz. Accordingly, if silica over-saturated igneous rocks and their derivatives from granodiorites through granites and pegmatites to hydrothermal veins are considered, the best qualities are mostly present in pegmatites and hydrothermal veins. Indeed, experience has shown that high-temperature igneous rocks produce poor-quality quartz in terms of structural impurities, whereas many pegmatites and some hydrothermal vein deposits, in general, produce better qualities. However, it is also clear that the concentration of impurities in igneous, hydrothermal and pegmatite quartz varies over several orders of magnitude and, therefore, parameters other than temperature also influence the incorporation of trace elements into the quartz-crystal structure. These other parameters are rarely addressed in the literature; however, the incorporation of Fe, for example, partially depends upon the oxidation state and hence the oxygen fugacity of the quartz-forming environment. The activity of other minerals may also influence the availability of some elements that may potentially be incorporated into the quartz-crystal structure. Finally, the trace element distribution in igneous quartz may follow the petrogenetic history of the quartz forming melt, as it is was documented in a recent study (Larsen et al. 2000) and is further substantiated in the work presented here.

4. ANALYTICAL STRATEGY

One of the main goals of the present project was to develop an *in situ* analytical procedure for the precise quantification of the trace element concentration in quartz. The preferred method is Laser Ablation High Resolution Inductively Coupled Plasma Mass Spectrometry (Fig 4) (LA-HR-ICP-MS). This is the only commercially available *in situ* method that consistently

may produce reliable results for quartz. This is because alternative *in situ* techniques either fail in obtaining the desired detection limits or fail because of insurmountable matrix effects (e.g. ion-probe). Given the novelty of the LA-HR-ICP-MS method, the unprecedented requirements for detection limits and precision of the desired isotopes and the absence of suitable standards, this activity grew in to the most important and time-consuming part of the project. In the end, it was necessary to rely on close collaboration with laboratories in both France (Université Paul Sabatier, Toulouse) and Australia (Monash University, Melbourne) before; finally, the method was fully developed at NGU.

The following outline begin with a popular summary of the LA-HR-ICP-MS method, is continued with a detailed account of the experimental approach that was finalized at NGU and is supplemented with the partial method that was conceived at Monash University (VIEPS). Finally, the pros and cons of the methods are evaluated in the conclusion.

4.1 Public summary of analytical approach

The LA-HR-ICP-MS method is a cutting edge analytical technique, which in its present form was introduced in the mid-nineties and currently is applied to geological samples by various factions of the Earth science community. This technique aim at estimating the trace element distribution in solid material (e.g. rock samples) with detection limits down towards 100 ppb and for certain elements, much lower still. The novel concept is to use a laser beam operating at the ultra violet (UV) wavelength (266 nm) to release microscopic samples from a rock surface. Because of the high energy of UV-light, the part of the sample bombarded by the laser-beam is partially melted and detached (i.e. ablated) from the sample surface (Fig 3) in an explosive process that ejects melt and dust into an argon-gas current sweeping through the sample chamber. Subsequently the ablated sample, which is suspended in the argon gas, is transported towards a magnetic mass spectrometer where the chemical composition is estimated. On the way to the mass spectrometer the sample passes through a torch system that generates argon plasma, i.e. a very high temperature medium maintaining a temperature of ca. 10 000°C. In passing this temperature regime the sample partially or fully decomposes to form positively charged ions (e.g. Ti^{4+} , Si^{4+} K^+). Continuing inside the mass spectrometer, the ions enter a strong magnetic field that bends the individual ions according to their energy, mass and charge hence different ions are aligned in distinctive trajectories throughout the magnetic field. After having passed through the magnetic field, a narrow slit is adjusted so

that only one specific trajectory, equivalent to the path followed by the desired ion (e.g. Ti^{4+}), will line up with the slit.

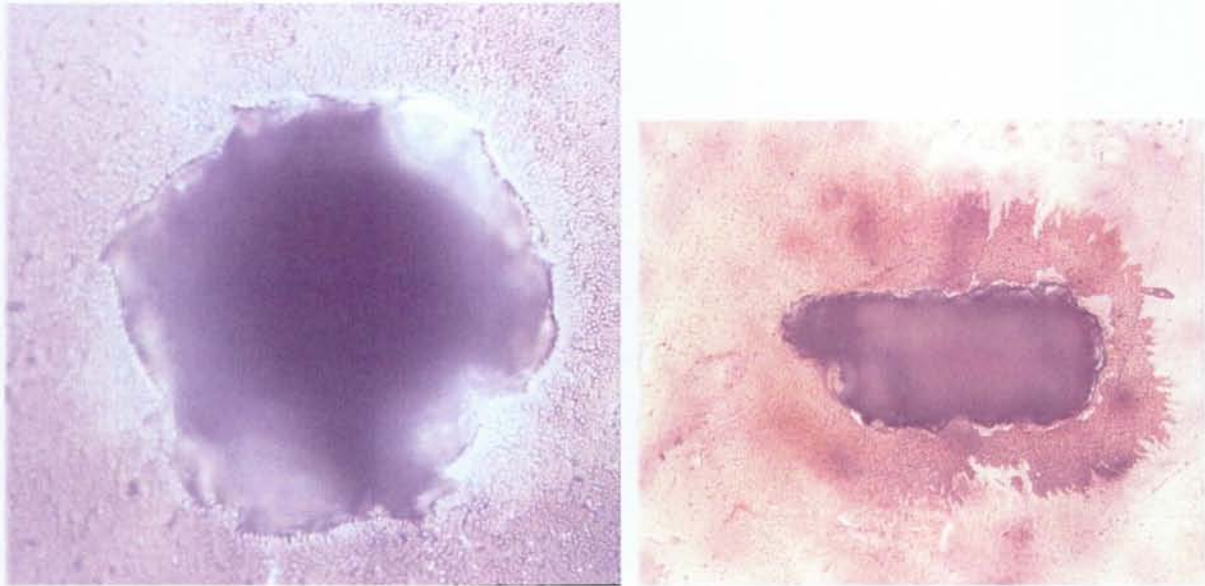


Figure 3: A) Ablation crater by *in situ* ablation of quartz with a beam diameter of $30\ \mu\text{m}$ that also corresponds to the approximate diameter of the crater; here shown in reflected light at high magnification. Notice how it is possible to identify individual sub- μm droplets of silicate melt along the crater rim. They were produced during the ablation. B) Ablation crater that in contrary to (A) was produced during ablation over an area in which the UV-laser operates according to a predefined grid. The crater shown on (B) was produced at Monash University and with approximate dimensions of $800 \times 350\ \mu\text{m}$, they are much larger than the 250×250 grids produced at NGU. The dark shadow surrounding the crater comprises silicate melts that were produced during the ablation process. C) Custom made quartz standards produced at NGU by M. Ødegård et al. (1998). The standards are ca. 5 mm in diameter. Dark areas are vesicles.



The ions that are allowed through the slit will subsequently collide with a detector system that measures the number of collisions per second (counts/sec), a number that is directly proportional to the concentration in the sample. One of the novel features of the mass spectrometers at NGU and VIEPS is their ability to rapidly sweep over large parts of the periodic table (Li^7 to U^{238}) and rapidly to change between Low-, Medium- and High Resolution (respectively LR, MR and HR). In LR mode, the width (i.e. atomic mass range)

over which a particular isotope is measured is quite wide, facilitating very low detection limits (down to the ppt level for some isotopes) and high precision. However, certain compounds having nearly equal masses, which may interfere with the measurements and invalidate the final result. Interferences may be avoided by narrowing the mass range over which the measurements are performed and, depending on the size and proximity of the interfering compounds, the measurement may be done in MR or HR mode. These options, although drastically reducing the sensitivity of the measurement, facilitates estimation of difficult isotopes such as for example K, Ca, S and As that rarely can be quantified with conventional mass spectrometric techniques.

The laser system which is used for ablation of the samples operates with a typical beam diameter of 10-100 μm a pulse energy of <30 mJ, and with a frequency of max 10 Hz (i.e. 10 shots/second) with a shot-duration of <10 ns. Either, laser sampling is performed in a single spot (Fig 3A) or in an area (raster) where the laser beam moves along a pre-defined grid (Fig 3B) and the final result reflects the average composition over the area.

Absorption of UV-laser light varies greatly from one sample to the next hence the volume of material that is ablated cannot be predicted. Therefore, quantification of an element in the sample requires that the concentration of one element is known already. This element is called the internal standard and, typically, is a major element in the mineral that either is known stoichiometrically, as for examples Si in quartz, or is estimated by another analytical method. The concentration of an unknown element in the sample is then compared to the intensity of the same element in a standard in which the concentration is known. Given this information, the unknown concentration may be quantified according to a well-known equation. Quantification of Ti in quartz, for example, where Si is used as an internal standard is expressed in the following way

$$C_{\text{Ti in sample}} = [C_{\text{Ti in standard}} / (I_{\text{Ti in standard}} / I_{\text{Si in standard}})] * [I_{\text{Ti in sample}} / I_{\text{Si in sample}}] * [C_{\text{Si in sample}} / C_{\text{Si in standard}}]$$

Where "C" is concentration in ppm and "I" is intensity in counts/second.

4.2 Experimental approach used at NGU

A standard double focusing, sector field, ICP-MS (Fig 4) (Finnigan MAT, ELEMENT) instrument is used (Giessmann & Greb, 1994, Feldmann et al. 1994). The configuration

included the CD-1 option from Finnigan, consisting of a torch-inserted module that replaced the standard Element ICP torch holder. The laser used for ablation was a Finnigan MAT-Spectrum, Berlin, Germany, UV laser. A description of the UV laser system can for example be found in Perkins and Pearce (1998). The laser was run with a shot frequency of 20 shots/s and 30 μm spot size on a raster not larger than maximum 250 x 250 μm . The ICP-MS instrumental operating parameters were tuned on ^{139}La in NIST612 to give maximum sensitivity and stability.



Figure 4: The picture above show the LA-HR-ICP-MS instrument at the Geological Survey of Norway. To the left, is the Finnigan MAT *ELEMENT* double focusing, sector field mass spectrometer. To the right is the Finnigan MAT-Spectrum UV-laser. The protection shield around the laser unit is open so that one may have a look into the sample chamber (black well on the white block), where the quartz samples are inserted before analysis. A tubing system (not visible) running behind the operator conveys the ablated material from the laser unit to the mass spectrometer.

Due to interferences for some ions, three mass resolutions were used for the analysis of the elements: Al, Ba, Be, Cr, Fe, Ge, K, Li, Mg, Mn, Pb, Rb, Sr, Th, Ti and U. Lithium Be, Al, Mn, Ge, Rb, Sr, Ba, Pb, Th, and U were successfully analysed in low resolution ($m/\Delta m=300$), whereas Mg, Ti, Cr, and Fe were analysed at medium resolution ($m/\Delta m\approx 3500$) and K at high resolution ($m/\Delta m>8000$) because of mass interferences at low- and medium resolution, respectively. The isotope, ^{29}Si , was used as internal standard at low resolution and ^{30}Si was used at medium and high resolution. External calibration was done by using the following international standards (Table 1): NIST612, NIST614, NIST616, BCS313/1(BAS), RGM-1(USGS), SRM1830 and BAM no.1 SiO₂ (Federal Institute for Material Research and Testing).

Standard and sample preparation

The SRM 1830 from National Institute of Standards & Technology (NIST) was cut into four sections of approximately 10x10mm to fit into the ablation chamber and the surface was abraded with diamond paste to enhance absorption of the UV-laser beam. The same was done with the BR-K1 and BR-FR2 from Breitländer, Germany.

The RGM-1 from USGS was melted in a graphite crucible under atmospheric pressure and 1200°C. To ensure homogeneity throughout the sample it was subsequently ground and melted again under the same conditions. The BCS313/1 and BAM no.1 SiO₂ from Federal Institute for Material Research and Testing was melted in a tantalum crucible under He/H₂ atmosphere at 2000 °C. Both the RGM-1, BCS313/1 and BAM no.1 SiO₂ were mounted in epoxy and polished. Concentrations of the relevant trace elements are summarised in Table 2.

Table 1 International standards used for calibration and their elemental concentrations.

Elements	NIST612	NIST614	NIST616	BCS313/1	RGM-1	SRM1830	BAM no.1 SiO ₂
	ppm	ppm	ppm	ppm	ppm	ppm	ppm
Li	41.54	1.74	0.91		57		0.25
Be	37.73	0.76	0.0221		2.4		0.1
Al	10582	10582	10582	190		635.1	8.7
Si							
Mn	38.43	1.37	0.58		278.8		0.03
Ge	34.64	0.95	0.32		1.3		0.4
Rb	31.4	0.855	0.1		150		0.007
Sr	78.4	45.8	41.72				0.013
Ba	37.74	3.29	2.4				0.05
Pb	38.57	1.85	1.85		24		0.05
Th	37.79	0.748	0.0252		15		0.009
U	37.38	0.823	0.0721		5.8		0.003
Mg	77.44	36.9	35.4	7.84			0.1
Ti	48.11	3.2	2.8			65.9	1.3
Cr	39.88	0.99	0.24		3.7		0.062
Fe	51	13.3	11	84		846.3	0.62
K	66.26		31.6			332	0.48

Table 2: New standard material applied to the present study.

Elements	SRM1830	BCS313/1	BRK1	BR FR2	RGM1
	µg/g	µg/g	µg/g	µg/g	µg/g
Li	7	27	36	82	71
Be	0.12	0.26	0.16	0.32	2.3
Al	624	298	166	12700	83800
Mn	11	1.9	0.3	6	273
Ge	0.4	0.4	1.6	0.5	1
Rb	0.5	0.5	0.1	10.6	154
Sr	49	1.7	0.2	6.3	
Ba	12	7.5	0.2	26.5	
Pb	0.9	1.6	0.2		24.4
Th	0.3	0.2	0.06	1.3	13
U	0.5	0.4	0.4	0.6	6.3
Mg		28.5	0.25	186	
Ti	58	101	4.4	373	
Cr	7	1.2	0.3	3.2	3
Fe	848	104	9.6	430	
K	294	64.5	< 5		

Calibration and measurement procedure

Each analytical run included 15 scans of all isotopes with a measurement time of each isotope adjusted to maximise the signal intensity. To avoid problems associated with signals (so called outliers) deriving from unstable ablation, a robust estimation method, Wilcox (1997) was used for identification of the correct signal. The advantage of this test is the high break down point at 0.5 that makes it attractive for outlier identification, (Staudte and Sheather, 1990). The median absolute deviation, ω , is defined by:

$$P(|X - x_s| \leq \omega) = .5$$

In other words, ω , is the median of the distribution associated with $|X - x_s|$ i.e. the distance between X and its median. (ω) is the .75 quartile of the standard normal distribution, which is approximately equal to .6745. The standard estimate of ω is the median absolute deviation statistic given by:

$$MAD = MED\{|X_1 - M|, \dots, |X_n - M|\}$$

where M is the common sample median. If observations are randomly sampled from a normal distribution, MAD does not estimate the standard deviation, (σ), but $z_{.75}\sigma$, where $z_{.75}$ is the .75 quartile of the standard normal distribution. MAD can be rescaled so that it estimates σ by:

$$MADN = \frac{MAD}{z_{.75}} \approx \frac{MAD}{.6745}$$

The outlier is then identified by:

$$z_i = \frac{x_i - M}{MADN}$$

If $z_i > z_{limit}$ where z_{limit} is usually chosen equal to 2.5 or 3 then x_i is an outlier.

An Ar-blank was run before each standard and sample. The background signal was subtracted from the response of the standard before normalisation against the internal standard. This was done to avoid memory effects between samples. Outliers were identified and removed from the background signal by the method described above. After normalisation against the internal standard, (S_i), the data was controlled for outliers and if z_i was larger than 3 then x_i was removed.

Standards used for calibration are listed in table 1 and 2 with certified mass concentrations, recommended concentration values, proposed and information concentration values taken from their respective certificates and from Goviaraju (1994), Nicholas et al. (1997) and Horn et al. (1997).

The actual number of standards included in each calibration calculations varied somewhat from one element to the next, (Table 1 &2, Appendix 1).

Calibrations were based on a linear relationship between normalised intensities (Y_i) and corresponding concentrations (X_i).

$$Y_i = \frac{I_i}{I_{S_i}} X_{S_i} \quad (1)$$

In equation (1) I_i and I_{S_i} are intensities for the analysed element and reference element (S_i), respectively, and X_{S_i} is the concentration of the reference element.

Weighted linear regression models were used for the calculation of the curve parameters. The weighted factors, w_i , were based on the square root of intensity for both analysed and reference element (S_i), see eq. (2).

$$s_{Y_i} \propto \tilde{s}_{Y_i} = Y_i \sqrt{\frac{1}{I_i} + \frac{1}{I_{Si}}} \quad (2a)$$

$$w_i = \frac{1/\tilde{s}_{Y_i}^2}{\sum \left[1/\tilde{s}_{Y_i}^2 \right] / n} \quad (2b)$$

In equation (2) s_{Y_i} are uncertainties in Y_i , \tilde{s}_{Y_i} are "expected" relationship for uncertainties in Y_i , w_i are the weighted factor and n are number of standards used in the regression analysis.

The used regression analyses are similar to that used by Ødegård et al. (1998) and further details can be found there. Figure 1 presents, as an example, the calibration curve for Fe⁵⁶.

Limits of detection (LOD)

Because of lack of a SiO₂ blank, 15 successive measurements on the BAM no.1 SiO₂ standard were applied to estimate the detection limits. Determination of LOD are based on 3 times standard deviation of the 15 measurements divided by the sensitivity, S :

$$LOD = \frac{3\sigma}{S}$$

Analytical uncertainties calculated from multiple analyses are summarized in Appendix 1.

4.3 Experimental approach used at VIEPS

The instrumental set-up used at VIEPS is virtually identical to the mass spectrometer and UV-laser used at NGU and thoroughly documented in Lahaye (1997). Table 4 summarises the analytical conditions and the following text mostly addresses the acquisition conditions at VIEPS where they differ from NGU.

During the analysis of quartz at VIEPS, both raster (ca. 800 x 400 μm) and single spot analysis were performed on doubly polished quartz wafers with a nominal thickness of 250 μm. Single spot and raster analyses were conducted with a repetition rate of 4 HZ, a laser energy of 0.1 mJ and with a laser diameter of 80 μm. Other instrument settings appear from Table 4. Analysis were conducted at both Low and Medium Resolutions although mass-drift in MR and, consequently, in HR modes appeared to be so serious that analysis at HR conditions were discontinued and in MR mode were very time consuming. Mass drift during MR and HR LA-analysis is a common problem encountered at many laboratories and, so far,

NGU maintains one of the few LA-HR-ICP-MS facilities that produce acceptable results during MR and HR analysis.

Table 4: Instrument settings and acquisition parameters

Laser Source	Merchantek LUV266, Q-switched Nd:YAG
Wavelength	266 nm
Repetition Rate	4 Hz
Energy	0.1 mJ
Crater Size	80 μ m
Methods	Single spot and raster (ca. 800 x 400 μ m)
Mass Spectrometer	Finnigan MAT ELEMENT HR-ICP-MS
Resolution	300
Cool Gas Flow	13.00
Auxiliary Gas Flow	1.10
Sample Gas Flow	1.20
Cone	High performance Ni
Sample Time	10 ms
Mass Window	22 %
Scan Type	EScan
Segment Duration	40 ms
Samples/Peak	15
Acquisition Points	3

^{29}Si was used as the internal standard and NIST612 was used for external standardization although in some of the runs custom made quartz standards (Ødegård et al., 1998) were also used. Of the isotopes included in the analysis (Table 2), NIST612 is only certified (by NIST) for Al, Si, Ca, Fe, Rb, Sr, Pb, Th, and U. The concentrations of other relevant isotopes (Li, B, Be, Mg, Sc, Ti, Cr, Mn, Cu, Ge, Y, Zr, Nb, Cs, Ba) are compiled from other sources (Pearce et al. 1997).

After initial test runs it was realised that Mn and B also had to be excluded from the element list because the best obtainable LOD's were several ppm, hence much above the maximum concentration reported for most quartz samples. Cu was excluded for the same reason in that the average LOD was well above 0.5 ppm. Table 5 summarises the elements that were finally included during analysis at Monash and compare with the results from NGU.

During both raster and single spot analysis the mass spectrometer performed 50 scans over the included isotopes. During the first 10 scans the background levels of each isotope was measured with the laser switched off. At the tenth scan the laser was switched on and the signal-intensity of each isotope was determined during the remaining 40 scans. Aluminium, Si and Ca were detected in analogue mode because the high concentration of these isotopes in the external standard otherwise would over-saturate the detector. All other isotopes were detected in counting mode. The mass window was fixed at 22% with 15 samples/peak in

order to get 3 channels per peak because this is the most efficient way in gathering laser ablation data with the Finnigan MAT ELEMENT instrument. Sample time was 0.01 s and the settling time was adjusted according to the length of the magnetic jump between each isotope (0.001 s per atomic mass unit and 0.005 s resting time) (Table 4).

After acquisition, the raw data were transferred to a separate PC for data processing. Initial data processing was performed using the custom-made software package known as *Schonbein* that currently is used only by VIEPS. The primary advantages of *Schonbein* is to rapidly select the desired parts of the spectrum for each isotope (background as well as analyte signal) and to rinse the signal for outliers and spikes derived from fluid and solid inclusions, microfractures, or other erratic fluctuations. Manipulation of the data in *Schonbein* is done in graphic interfaces so that the results of spike removal and data selection can be verified instantaneously. Subsequent statistical data management and calculation of LOD's, precision and analyte concentrations are performed by macros in Excel spreadsheets.

Table 5: Isotopes and acquisition conditions at VIEPS and NGU. i) Industrially important, (Yes) not yet included in NGU-method but may be included if desired.

Isotope	i	Main interferences	Resolution/remarks	Included at VIEPS	Included at NGU
⁷ Li	•	None	LR	Yes	Yes
⁹ Be		None	LR	Yes	Yes
¹¹ B	•	None	LR	No	Yes
²³ Na	•	Li-O	Air contamination	No	No
²⁵ Mg	•	Li-O	MR	No	Yes
²⁷ Al	•	None	LR	Yes	Yes
²⁹ Si	•	None	LR	Yes	Yes
³⁰ Si	•	N-O	MR and HR	No	Yes
³¹ P	•	N-O	Difficult to ionise	No	Maybe later
³⁹ K	•	Ar-H	HR	No	Yes
⁴⁴ Ca	•	Si-O	MR	Yes (at LR)	Yes
⁴⁷ Ti	•	Ar-Li	MR	No	Yes
⁴⁸ Ti	•	Ca ⁴⁸	MR	Yes (at LR)	No
⁵² Cr	•	Ar-O, Ar-N	MR	Yes (at LR)	Yes
⁵⁵ Mn	•	None	LR	No	Yes
⁵⁶ Fe	•	Ar-O, Ca-O	MR	No	Yes
⁵⁷ Fe	•	None	LR (Low abundance)	Yes	No
⁶³ Cu	•	None	LR	Yes	(Yes)
⁷² Ge	•	Ar-Ar (uncertain)	MR	Yes (at LR)	No
⁷⁴ Ge	•	None	LR	No	Yes
⁸⁵ Rb	•	None	LR	Yes	Yes
⁸⁸ Sr		None	LR	Yes	Yes
⁸⁹ Y		None	LR	Yes	(Yes)
⁹⁰ Zr		None	LR	Yes	(Yes)
⁹³ Nb		None	LR	Yes	(Yes)
¹³³ Cs		None	LR	Yes	(Yes)
¹³⁷ Ba		None	LR	Yes	No
¹³⁸ Ba		None	LR	No	Yes
²⁰⁸ Pb	•	None	LR	Yes	Yes
²³² Th		None	LR	Yes	Yes
²³⁸ U	•	None	LR	Yes	Yes

A more thorough account of the method developed at VIEPS for the analysis of quartz may be found in Larsen and Lahaye (1999):

5. COMPOSITION AND GEOLOGICAL SETTING OF PEGMATITE QUARTZ

5.1 Geological setting

Granite pegmatites in Setesdalen and Froland comprise classical chamber pegmatites, which in most examples crystallised as sub-vertical dikes (Fig5B) or sills (Fig 5A) (e.g. Bjørlykke 1935). They rarely exceed 20 metres in thickness and most pegmatites have an exposed lateral extension of less than 100 m although the economically important Gloserheia (Åmli, 1977) and Glamsland pegmatites are examples that extend for hundred of m in lateral dimensions. Although the tectonic and lithological settings differ strongly between Setesdalen and Froland, most pegmatites developed in mafic host rocks comprising amphibolite, norite and mafic gneisses. Granite pegmatites are extremely coarse-grained with individual crystals, in the interior parts varying in size from dm to m (Fig 5A). The pegmatites are strongly zoned, typically comprising a wall zone, one or several intermediate zones and one or several core zones that evolved in the innermost and/or upper parts of the pegmatite (Fig 6A). Some bodies may also contain a more fine-grained contact zone (Fig 5A). Textural and modal criteria are applied to distinguish between the individual zones and, in the present study, are based on own field observations together with earlier studies. When present, the contact zone, or chilled margin, is composed of relatively fine-grained perthitic feldspar, plagioclase, quartz, biotite and minor muscovite. The wall zone is dominated by dm size K-feldspar and plagioclase, accessory biotite and muscovite, and little or no quartz. In some examples, the wall zone is mostly composed of plagioclase with minor quartz and biotite (Fig 5A). The wall zone has a well defined or a gradual boundary towards the intermediate zone(s) (Fig 5A), which may vary considerably when comparing different pegmatites. Often, the intermediate zone begin with dm to m size blades of biotite that nucleates on the boundary between wall zone and intermediate zone and radiate towards the interior of the pegmatite (Fig. 5B). Potassic macro-perthitic feldspar, plagioclase and quartz are interspersed in near equal volumetric proportions between biotite and muscovite. In most pegmatites, and in all the pegmatites included in this study, biotite is the dominant mica. The first intermediate zone may gradually develop in to an intermediate zone with even more coarse-grained K-feldspar and plagioclase and quartz with biotite being absent or scarce. Often this 2nd intermediate zone develops spectacular examples of graphic granite with distances between quartz and

feldspar domains of several dm (Fig 5B). Finally, the 2nd intermediate zone gradually develops into the core zone that may be entirely composed of quartz but often

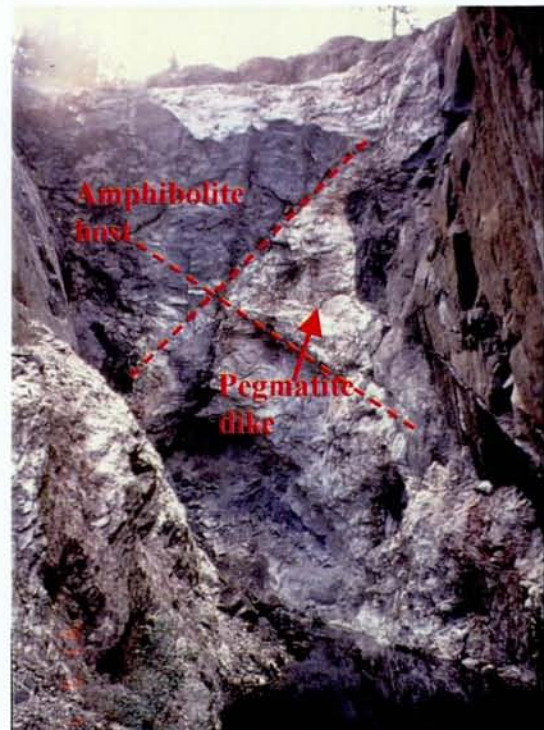
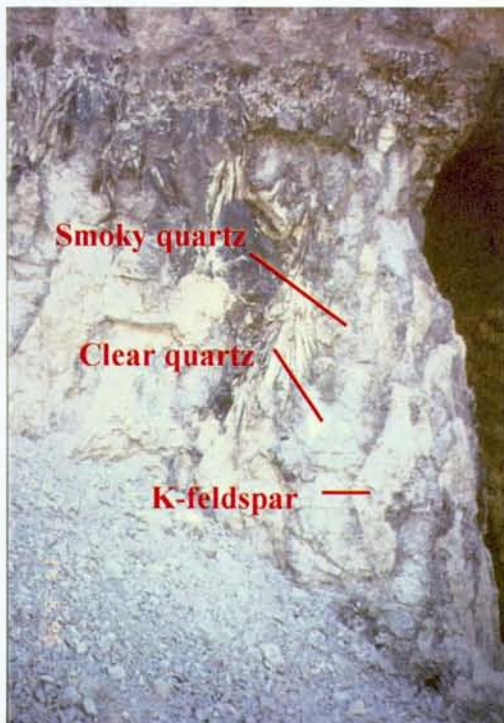
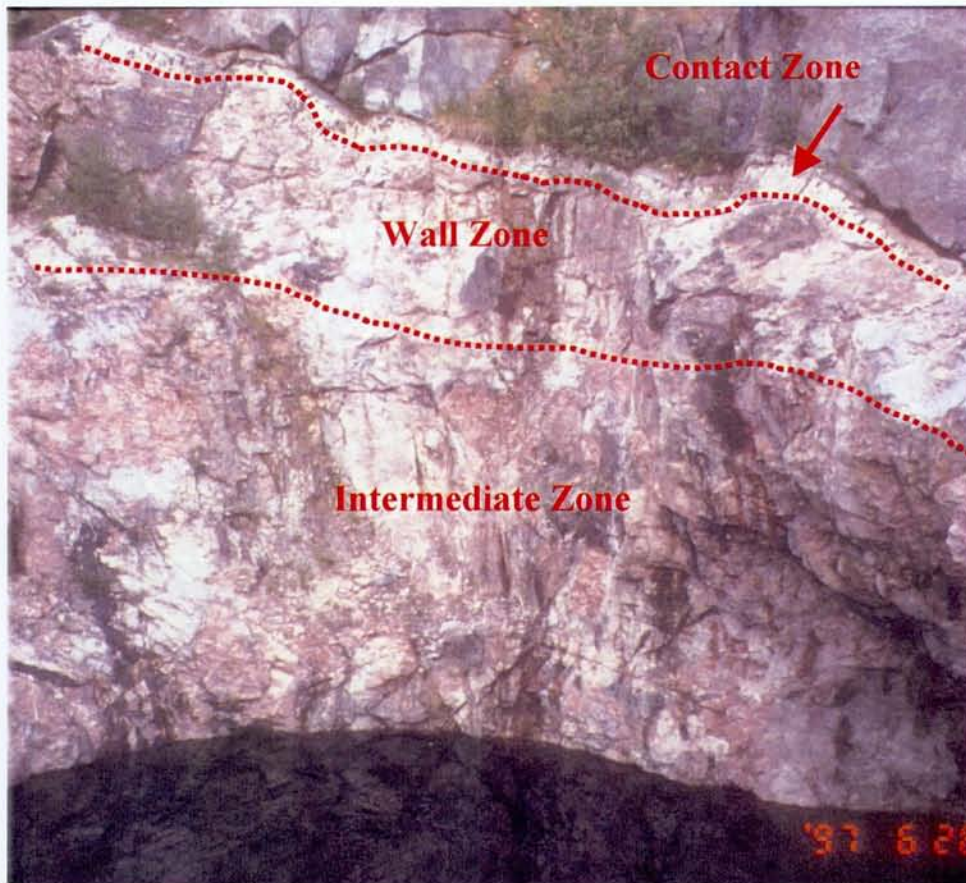


Figure 5: Geometry and zoning patterns of granite pegmatites in Evje-Iveland. A) Large pegmatite sill that intruded in an amphibolite host rock. K-feldspar is red, plagioclase may be most easily recognized as yellowish white areas in the wall zone, quartz is white. B) Relations between smoky quartz, clear quartz and K-feldspar in IZ. Note also the radiating blades of biotite extending from the top of IZ. C) Erratic pegmatite dyke intersecting amphibolite host rock. Note that the pegmatite is constrained by divergent fault systems.

contain rafts of K-feldspar and minor plagioclase floating in the quartz masses (Fig 6A).

Larger pegmatites develop several quartz zones in the interior portions, which are separated by walls of intermediate zone minerals. Other than the zones described above, some pegmatites develop a narrow 3rd intermediate zone, which is entirely composed by K-feldspar and, in rare examples, some pegmatites features repetitive evolution of the first intermediate zone with radiating aggregates of biotite.

Other than perthitic K-feldspar, plagioclase, quartz, biotite and white mica, the dominant primary magmatic phases in the Setesdalen and Froland pegmatites includes magnetite, spessartite garnet, monazite, beryl, xenotime, euxinite, fergusonite and gadolinite (Andersen 1921, 1931; Bjørlykke, 1935; Åmli, 1975, 1977). Clevelandite, microlite and tantalite typically formed from late hydrothermal solution replacing primary magmatic minerals in cavities and along fractures intersecting the pegmatites. However, hydrothermal replacement features are uncommon in both Evje-Iveland and Froland (Bjørlykke 1935; Fought 1993; Stockmarr, 1994). Recent studies document that late magmatic volatiles in Setesdalen comprises medium salinity H₂O-CO₂-NaCl fluids with 10-15 vol% CO₂ or low salinity H₂O-CO₂-NaCl-MgCl₂-FeCl₂ fluids with 5-10 vol% CO₂ (Larsen et al., 1998) (Fig 6B). Garnet dominates the outer parts of the intermediate zone and monazite, xenotime, fergusonite and euxinite are nearly always associated with- and probably nucleated on blades of biotite at the transition between wall-and intermediate zones (Bjørlykke 1935). Together, this indicates that these phases formed early during crystallization of the pegmatites whereas gadolinite and beryl formed from the last fractions of pegmatitic melt (Bjørlykke, 1935).

Detailed descriptions of the minerals composing pegmatites in Setesdalen and Froland, may be found in the comprehensive studies of Bjørlykke (1935), Åmli (1975, 1977) and references therein.

Quartz

Quartz is common throughout the pegmatites and, in quantity, is inferior only to K-feldspar. Most of the quartz is transparent although in places it may be milky-white due to high abundances of micro-fractures or, in rare cases, to high densities of fluid inclusions. Pale grey smoky quartz is particularly common throughout the wall and intermediate zones and always occurs in 10-15 cm-wide rims enclosing feldspar (Fig 5B). Quartz that occurs at distances greater than 15 cm from feldspar is milky-white or transparent (Fig 5B). Accordingly, it is implied that the smoky colour of quartz is a result of γ -radiation from decaying radioactive

elements in feldspars, rather than being a consequence of radiogenic elements from structural or solid inclusions incorporated in the quartz.

Microscopic examination of quartz shows that solid inclusions other than rutile are rare, although magnetite may be present in some of the pegmatites. Rutile is common in intermediate-zone quartz but rare in the core-zone and occurs as minute μm to sub- μm thick needles that are evenly dispersed throughout the quartz.

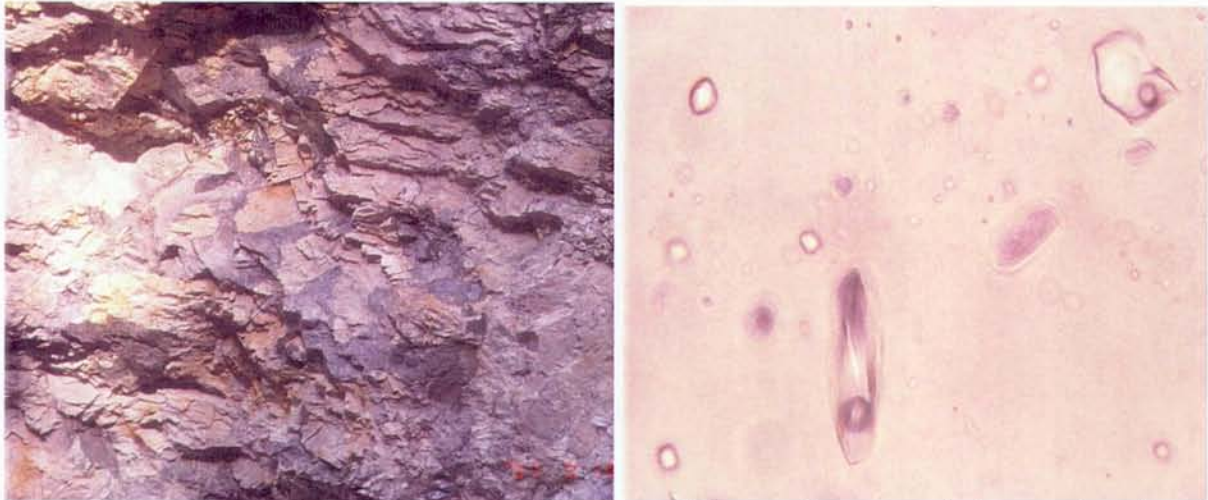


Figure 6: Pegmatite dike from Froland. A) Detail from one of the several core zones in the central portions of the pegmatite dike, ca. 1 metre from edge to edge. Pale yellow minerals are euhedral K-feldspar and grey minerals are smoky quartz. B) Low salinity fluid inclusions from the core zone. The fluids are three phase inclusions comprising of (1) liquid low salinity H₂O, (2) liquid CO₂ plastered to the wall of the vapour bubble and (3) gaseous CO₂ in the central portions of the bubble. Largest inclusion is ca. 12 μm on long axis.

5.2 Trace element distribution in quartz

Quartz from the intermediate and core zones of granite pegmatites was analysed for Li, Al, Be, Mg, K, Ti, Cr, Mn, Fe, Ge, Rb, Sr, Ba, Pb, Th, and U (Table 6). After calculating the concentration of Na by the equation outlined above, this spectrum of elements includes the most important species that occur as structural impurities in quartz. A complete list should also include Ca, B, and P, however, as previously outlined, these elements cannot presently be quantified but may be included in coming analytical procedures.

The most important substitutional impurities (replacing Si^{4+}) comprise Al, Ti, Fe and Ge whereas the most common charge compensators includes Li, Na and K. Together these elements comprise 95 wt% of the impurities in quartz and Al and Ti dominates with normally tens of ppm (Table 6).

Table 6: LA-HR-ICP-MS analysis of quartz, all concentrations in ppm. CZ: Core zone. IZ: Intermediate zone. *)Outliers, not included in calculation of average

Sample	UTM-E	UTM-N	Locality	Zone	Pegmatite field	Na(calc.)	Li	Al	Be	Mg	K	Ti	Cr	Mn	Fe	Ge	Rb	Sr	Ba	Pb	Th	U
RBL 97016	434400	6474225	80	CZ	Evje-Iveland	0.0	13.2	33	0.294	<1.9	35.7	11.6	<0.17	1.14	29.2	2.71	0.508	0.51	0.25	0.58	0.037	0.273
RBL 97023	434300	6475200	81	CZ	Evje-Iveland	11.1	16.0	75	<0.12	*31.8	nd	26.8	1.46	1.48	84.2	3.46	0.531	1.32	3.23	0.74	0.043	0.230
RBL 97026	434475	6475550	82	CZ	Evje-Iveland	0.0	17.0	36	0.353	<1.9	131	17.2	<0.17	0.13	12.7	1.64	0.556	0.47	1.44	1.01	0.106	0.544
RBL 97030	434650	6476725	83	CZ	Evje-Iveland	23.1	11.0	70	0.357	<1.9	15.1	26.5	<0.17	0.55	12.2	1.84	0.334	0.71	1.55	<0.18	0.097	0.567
RBL 97032	436150	6477500	84	CZ	Evje-Iveland	47.0	28.0	164	0.712	15.9	45.0	50.5	<0.17	*4.93	10.9	5.63	2.340	1.69	*122	*11.30	<0.010	<0.140
RBL 97036	435750	6478050	85	CZ	Evje-Iveland	0.0	<19.0	61	<0.12	15.8	22.3	34.0	<0.17	<0.12	3.97	1.84	0.106	<0.12	3.02	1.33	<0.010	0.151
RBL 97041	435675	6478700	86	CZ	Evje-Iveland	0.0	21.0	75	<0.12	29.7	176	53.1	<0.17	0.47	12.0	1.02	1.120	2.39	*85.20	*7.76	0.072	0.289
RBL 97045	435400	6481750	87	CZ	Evje-Iveland	16.1	17.0	85	<0.12	2.7	18.8	38.0	<0.17	2.41	22.7	1.15	0.463	0.53	0.230	0.23	0.047	0.298
RBL 97052	433350	6483750	88	CZ	Evje-Iveland	0.0	<19.0	58	0.337	18.0	47.4	48.6	<0.17	1.22	7.05	1.51	1.210	*4.19	*153.0	*16.90	0.145	<0.140
RBL 97059	435350	6485500	90	CZ	Evje-Iveland	0.0	18.0	43	0.210	<1.9	10.4	21.1	<0.17	0.50	12.6	2.35	0.094	0.51	0.92	0.55	0.113	0.302
RBL 97066	436575	6486150	91	CZ	Evje-Iveland	10.3	<19.0	86	0.328	<1.9	38.0	31.6	<0.17	0.87	7.6	1.54	0.412	0.40	<0.17	0.37	<0.010	0.215
RBL 97070	437175	6488600	92	CZ	Evje-Iveland	20.5	22.0	110	<0.12	<1.9	20.9	22.3	0.199	0.33	3.8	2.31	0.225	0.41	0.32	0.33	0.035	0.154
RBL 97077	436500	6489800	93	CZ	Evje-Iveland	61.5	<4.6	90	0.522	5.3	9.32	27.3	<0.170	<0.12	<4.7	2.47	<0.080	0.43	0.39	<0.18	<0.010	<0.140
RBL 97084	432950	6491350	94	CZ	Evje-Iveland	0.0	18.0	<19	0.277	10.2	48.8	18.4	<0.170	<0.12	9.9	0.67	0.686	0.41	6.90	0.60	0.029	0.156
RBL 97088	436070	6494175	95	CZ	Evje-Iveland	0.0	15.0	<19	0.208	<1.9	30.0	56.9	<0.170	0.88	13.1	1.66	0.406	0.65	0.21	<0.18	0.028	0.218
RBL 97093	437900	6495750	96	CZ	Evje-Iveland	9.8	22.0	97	<0.12	<1.9	<5.3	45.4	<0.170	<0.12	8.4	1.92	<0.080	0.12	0.51	<0.18	0.110	<0.140
RBL 97097	437850	6497075	97	CZ	Evje-Iveland	35.0	<4.6	59	<0.12	<1.9	<5.3	36.1	<0.170	<0.12	5.6	1.40	0.403	0.34	0.33	<0.18	0.041	0.168
RBL 97104	461350	6479125	99	CZ	Froland	*130	5.6	*175	0.658	<1.9	74.5	39.3	<0.170	0.58	3.8	3.12	0.350	0.75	1.02	0.25	0.032	<0.140
RBL 97109	466900	6487500	100	CZ	Froland	0.0	12.0	<19	<0.12	<1.9	42.1	13.6	<0.170	<0.12	6.7	3.58	0.119	0.43	12.3	1.35	0.045	0.164
RBL 97113	466200	6488350	101	CZ	Froland	1.0	<4.6	<19	0.363	<1.9	<5.3	9.0	<0.170	<0.12	4.7	1.37	<0.080	0.08	0.10	<0.18	<0.010	0.204
RBL 97120	467325	6494850	103	CZ	Froland	1.0	<4.6	<19	0.132	<1.9	5.76	9.0	<0.170	<0.12	5.1	1.47	0.370	0.14	0.14	<0.18	<0.010	<0.140
RBL 97130	469350	6495125	108	CZ	Froland	9.5	<4.6	29	<0.12	*45.1	21.6	42.5	<0.170	0.58	10.5	2.31	0.332	0.89	1.27	2.49	0.030	<0.140
RBL 97132	469375	6495250	109	CZ	Froland	1.0	<4.6	<19	0.272	3.9	25.0	10.5	<0.170	0.16	2.8	2.55	0.187	0.51	4.89	3.43	<0.010	<0.140
RBL 96004	436400	6494700	96-1	IZ	Evje-Iveland	47.7	<19.5	132	0.863	7.7	*448	84.5	0.301	2.71	81.8	2.01	1.980	1.46	7.04	*3.67	0.258	0.796
RBL 96006	436300	6494700	96-2	IZ	Evje-Iveland	nd	nd	nd	<0.12	<1.9	80.3	54.0	<0.170	1.58	27.9	2.41	0.963	0.65	0.79	0.77	0.084	0.773
RBL 96007	437100	6495325	96-3	IZ	Evje-Iveland	nd	nd	nd	<0.12	<1.9	320.0	47.4	0.348	1.56	38.1	2.21	0.873	1.03	2.12	0.93	0.301	0.796
RBL 96008	437050	6496000	96-4	IZ	Evje-Iveland	nd	nd	nd	0.356	<1.9	20.0	103.0	<0.170	1.54	36.9	2.02	0.134	0.94	0.91	0.37	0.242	0.588
RBL 96012	433500	6483975	96-5	IZ	Evje-Iveland	12.0	<4.6	32	0.536	11.6	*1750	63.1	0.450	3.25	35.6	3.22	0.641	2.92	0.83	1.66	0.244	1.080
RBL 96014	433275	6488275	96-6	IZ	Evje-Iveland	10.1	<4.6	30	<0.12	13.8	319.0	36.1	0.936	2.22	34.7	3.97	*4.450	1.05	1.26	<0.18	0.082	0.591
RBL 96016	433500	6484250	96-7	IZ	Evje-Iveland	4.1	<4.6	23	<0.12	<1.9	36.7	44.1	0.217	0.67	25.6	2.79	0.897	1.28	1.04	0.83	0.053	1.040
RBL 96017	433600	6485500	96-8	IZ	Evje-Iveland	12.0	<4.6	32	0.341	10.4	*1170	17.9	0.733	1.53	11.8	4.24	0.239	1.45	1.82	0.51	0.114	0.803
RBL 96019	428425	6495525	96-9	IZ	Evje-Iveland	63.7	<4.6	93	0.520	<1.9	22.0	45.8	<0.170	0.93	11.1	1.26	0.550	0.96	1.08	0.23	0.064	0.589
RBL 97022	434300	6475200	96-10	IZ	Evje-Iveland	9.2	<4.6	29	0.218	<1.9	25.9	47.3	<0.170	0.25	30.4	<1.90	<0.080	1.15	0.50	<0.18	<0.010	0.318
Average CZ Evje-Iveland						13.8	16.7	69.4	0.262	7.1	41.2	33.3	<0.170	0.66	15.3	2.1	0.561	0.69	1.39	0.475	0.056	0.242
Average IZ Evje Iveland						22.7	<4.6	52.8	0.333	5.5	117.7	54.3	0.367	1.62	33.4	2.6	0.706	1.29	1.74	0.629	0.145	0.737
Average CZ Froland						2.5	<4.6	<19	0.279	<1.9	29.0	20.7	<0.170	0.28	5.6	2.4	0.239	0.47	3.29	1.314	0.023	<0.14

42

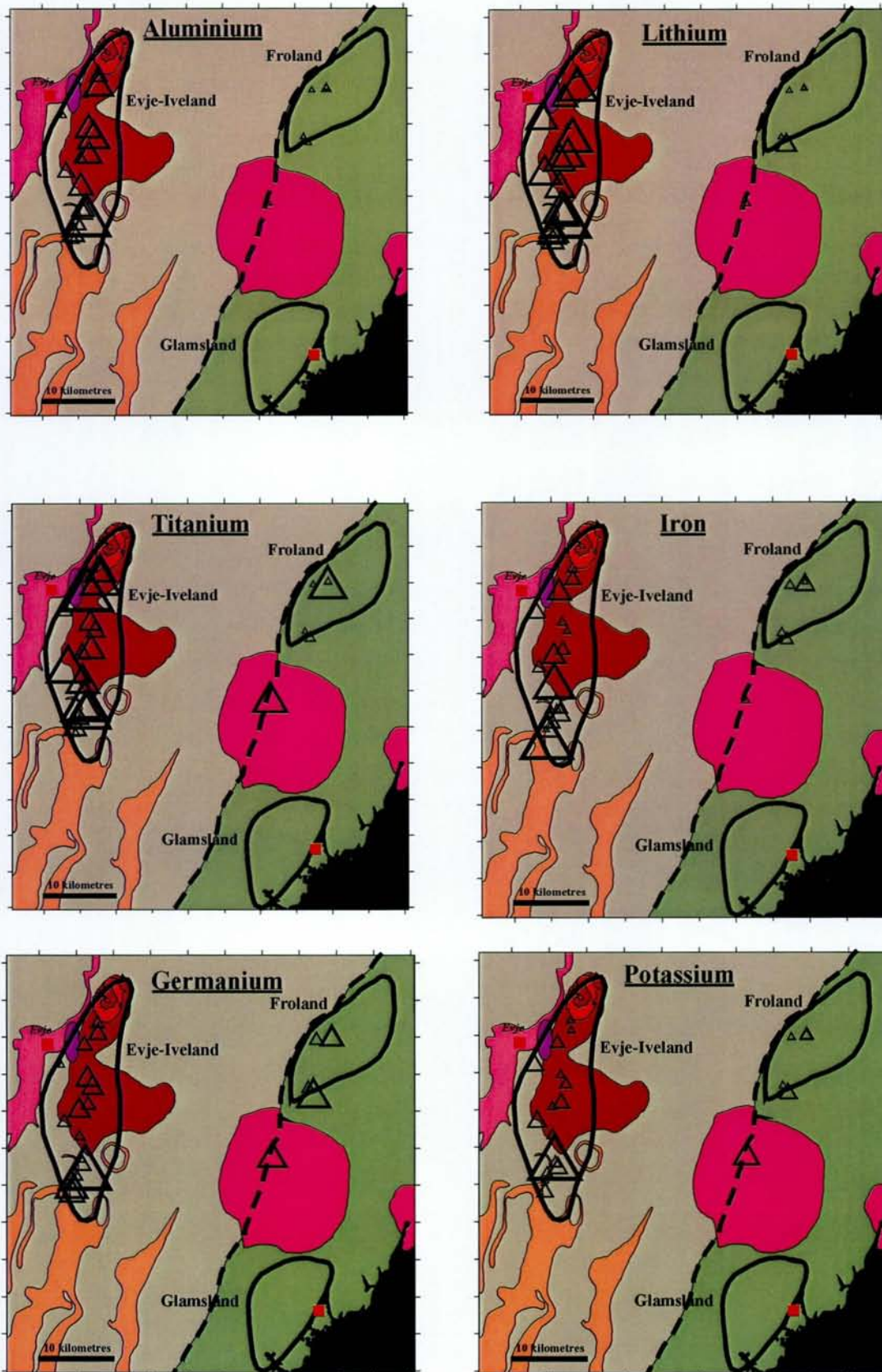


Figure 7: Areal distribution of trace elements in quartz from the core zone of granite pegmatites. Each figure demonstrates the relative concentration of one element from a specific pegmatite locality. The size of the triangles is proportional to the total concentration of the element. The elements shown on this figure comprises >95 wt% of the trace impurities in quartz and, except for K, they are predominantly structural bound elements. Note the relatively high purity of Froland quartz. Basement geology after Pedersen (1981), Falkum (1982) and Padgett & Maijer (1994).

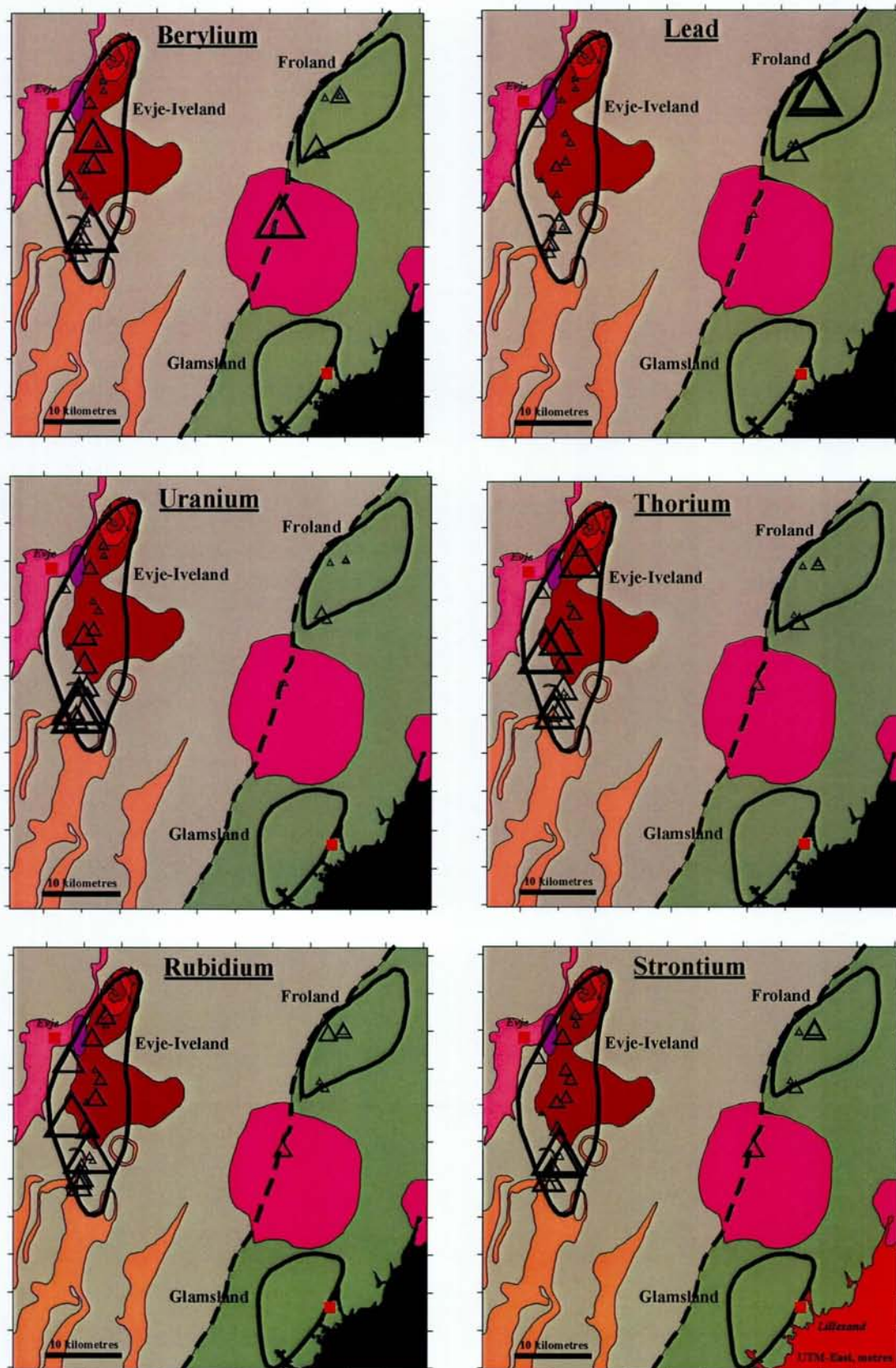


Figure 8: Areal distribution of trace elements in quartz from the core zone of granite pegmatites. Each figure demonstrates the relative concentration of one element from a specific pegmatite locality. The sizes of the triangles are proportional to the total concentration of the element. Figure 7 show the distribution of some of the minor trace impurities that together comprises <5 wt% of the trace elements in quartz.

The total average concentration of trace elements in quartz is 203 ppm in core-zone quartz from Evje-Iveland, 301 ppm in intermediate zone quartz from Evje-Iveland and 92 ppm in the core zone quartz from Froland. Accordingly, the Froland quartz is significantly more pure than Evje-Iveland quartz.

Looking more closely at the data, it appears that Core Zone (CZ) quartz from Evje-Iveland, on the average, features a distinctively different trace element distribution than Intermediate zone quartz (IZ) (Table 6). Core zone quartz has significantly higher concentrations of Li and Al, whereas all other elements (Be, K, Ti, Cr, Mn, Fe, Ge, Rb, Sr, Ba, Pb, Th, U) are markedly enriched in IZ and, largely, yields twice the concentrations of CZ-quartz.

Looking at key elements and their regional distribution in CZ-quartz from Evje-Iveland and Froland, several significant features emerge (Fig 7 & 8). Again it is clear that the concentration of most of major trace impurities, including Al, Li, Ti and Fe (Fig. 7) is highest in the Evje-Iveland district. Potassium (K) on the average yields lower concentrations in Froland, however, many localities in Evje-Iveland are also low in K (Fig. 7) and, occasionally, produce even lower concentrations of what has so far been recorded in Froland.

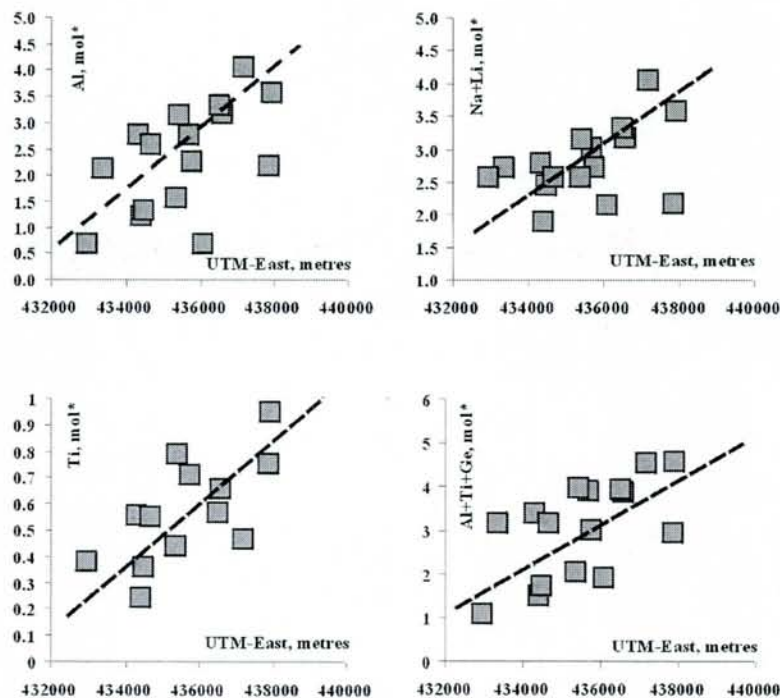


Figure 9: Distribution of structural impurities in core zone and intermediate zone quartz from Evje-Iveland, plotted as a function of geographical distribution relative to the UTM-East coordinates. East is towards left in the figures. The figures includes ca. 90 wt% of the structural impurities in quartz and imply that the Al, Ti, Ge, Li and Na concentrations fall towards West in the Evje-Iveland pegmatite field.

Germanium is another significant trace impurity that is not preferentially enriched in any of the pegmatite fields (Fig 7). Among the minor trace impurity elements (Fig 8) Froland produces significantly lower concentrations, of both Rb, Sr, Th and U (Fig. 8) whereas Pb is clearly enriched in Froland. Beryllium is not preferentially enriched in any of the areas.

Besides for conspicuous differences in the trace-element distribution between Froland and Evje-Iveland, systematic differences are also implied internally in the Evje-Iveland district. Accordingly, the concentration of Al, Ti, Ge, Na and Li decreases towards West (Fig 9). The molar concentration of the substitutional impurities, Al, Ti and Ge falls to less than a third when going towards west and is associated with a comparable decrease in the charge compensator elements Na and Li. Minor elements including Sr, Rb, Th, Mn and Mg decrease when going towards East.

6. DISCUSSION

6.1 Analytical strategies

Evaluation of the results obtained at VIEPS and NGU, respectively, imply that analysis of Al and Li was most successful at VIEPS whereas the analysis of Be, Mg, K, Ti, Cr, Mn, Fe, Ge, Rb, Sr, Ba, Pb, Th and U produced more reliable result by using the analytical method developed by NGU. Calcium (Ca), presents a special problem in that reliable standards containing this element at the ppm and sub-ppm level do not currently exist. However, when NGU-manufactured standards are available, Ca may be included in the analytical package. Boron presents a different problem in that although the analysis of this element should be fairly unproblematic in reality, however, the response signals from this element were erratic and inconsistent and contained a high density of spikes. The problems with B could be a simply matter of contamination from the tubing system or improper cleaning of the sample surface. Pre-ablation of the upper 10-20 μm of the sample surface may solve the problem. Sodium (Na) cannot currently be analysed by the LA-method because the concentration of this element in the air, which is partially introduced together with the argon carrier gas, amounts to several hundreds ppm. However, for most quartz it may be assumed that the following equation, expressing the molar concentration of structurally bound Al, Li and Na in igneous quartz and most hydrothermal quartz, is valid (e.g. Dennen, 1964, 1967)

$$[\text{Al}] = [\text{Li}] + [\text{Na}] \text{ (in mol\%)}$$

Accordingly, the concentration of Na may be approximated if the concentration of Al and Li is known. This approach may suffice for many applications. Phosphorous (^{31}P) may in theory

be analysed in MR-mode, however, this ion is difficult to properly ionise and only irrelevantly high LOD's can be obtained.

6.2 Composition of quartz compared to granite pegmatite evolution

Other than quartz, K-feldspar co-existing with quartz was also sampled in order to address petrogenesis of the granite pegmatites from Evje-Iveland and Froland. A separate publication addressing the chemistry of K-feldspar and how it relates to granite pegmatite petrogenesis is near completion (Larsen, *in prep*). Although the granite pegmatites in Evje-Iveland and Froland share many similarities in mineralogy, age and origin, these studies imply that granite pegmatites from Froland and Evje-Iveland were derived from significantly different source magmas. The study also demonstrates that K-feldspar reflects the REE-chemistry of the melt and efficiently distinguishes between more or less evolved granite pegmatites. Important for the present study of quartz, is the strong coherence between the chemistry of K-feldspar and the evolution/petrogenesis of granite pegmatites. For example, it is implied that the concentration of K, Ca, Sr, Ba and LREE decrease with differentiation of the granite pegmatite liquid whereas the content of Rb, Ga, Pb and HREE are increasing. A handful of studies from other pegmatite fields in the world also document that K, Ca, Sr, and Rb and Pb varies systematically with differentiation in featuring the same trends as those that are identified in Evje-Iveland and Froland (e.g. Cerny & Meintzer, 1988; Shearer et al., 1992). However, that the REE distribution in K-feldspars is also strongly controlled by igneous differentiation was not realised until now (Larsen *in prep*).

Having established that K-feldspar changes (Larsen, *in prep*) with the melt evolution in both Evje-Iveland and Froland, it is meaningful to compare the trace-element composition of quartz with the chemistry of K-feldspar. And not least to evaluate if sampling and analysis of granite pegmatite K-feldspar may be applied in exploration after high-purity quartz deposits, but also to define some of the principles that governs the purity and trace element distribution of quartz during igneous processes.

To evaluate if the chemistry of quartz is governed by igneous differentiation of the pegmatite forming melts, the Ti-concentration in quartz is probably one of the best parameters to study. Ti almost exclusively act as a substitutional impurity, with a charge of 4^+ is independent of the activity of charge compensators and, finally, Ti may be quantified with high precision and low detection limits with the LA-HR-ICP-MS method.

Figure 10 show the most important results regarding the concentration of Ti as a function of various elements in K-feldspar. As a first observation, it is implied, indeed, that the concentration of Ti in quartz is falling parallel with an increase in the concentration of Dy and Er (Fig. 10A & B) in K-feldspar. Dy and Er comprise the two HREE in K-feldspar that yield the highest concentrations and, therefore, obtain better precision during analysis than the other HREE. As previously mentioned, the HREE contents of K-feldspar yield progressively higher concentrations as the granite pegmatite melts become more evolved. Accordingly, it is implied that the concentration of Ti in quartz decreases with differentiation of the granite pegmatite melt. The concentration of Ti in quartz may also be compared with the anorthite component and with the total concentration of Ca and Sr in K-feldspar. The anorthite, Ca and Sr concentrations in K-feldspar decrease with differentiation and, it appears, the concentration of Ti in quartz is also decreasing together with these elements. Again, the link between Ti in quartz and differentiation is supported.

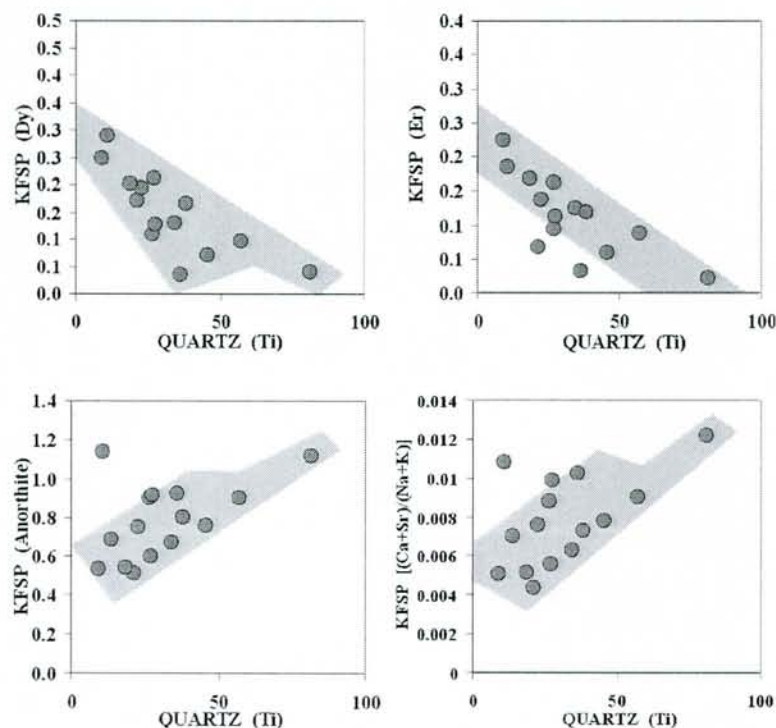


Figure 10: Concentration of a substitutional impurity in core zone and intermediate zone quartz and K-feldspar from both Evje-Iveland and Froland. The concentrations of various elements in K-feldspar are shown on axis to the left whereas the concentration of Ti in co-existing quartz is marked on the bottom axis. See text for further explanations.

The Ti-content of quartz also follows several other elements in K-feldspar as for example Y that overall follows the behaviour of HREE.

Li and Na (which of course is calculated, not analysed), to take the two most important charge compensators in quartz, also show distinctive correlations with the HREE, Sm, Y and the anorthite contents of K-feldspar (Fig. 11). However, recalling the analytical difficulties when it comes to Li, the data points are somewhat more scattered. Still, however, when compared to co-existing K-feldspar, the concentration of Y and HREE is decreasing parallel with an increase in Na+Li (Fig. 11A & B). On the contrary, the concentration of Na+Li is increasing parallel with the concentration of Anorthite and Sm in K-feldspar (Fig. 11C & D). As well as with Ti, it is implied that the concentration of charge compensator elements in quartz are controlled by differentiation of the pegmatite forming melts.

Finally, the distribution of Al also implies that the concentration of this element is falling in progressively more differentiated pegmatite melts, although, the analytical difficulties previously outlined obstruct a full evaluation of this element.

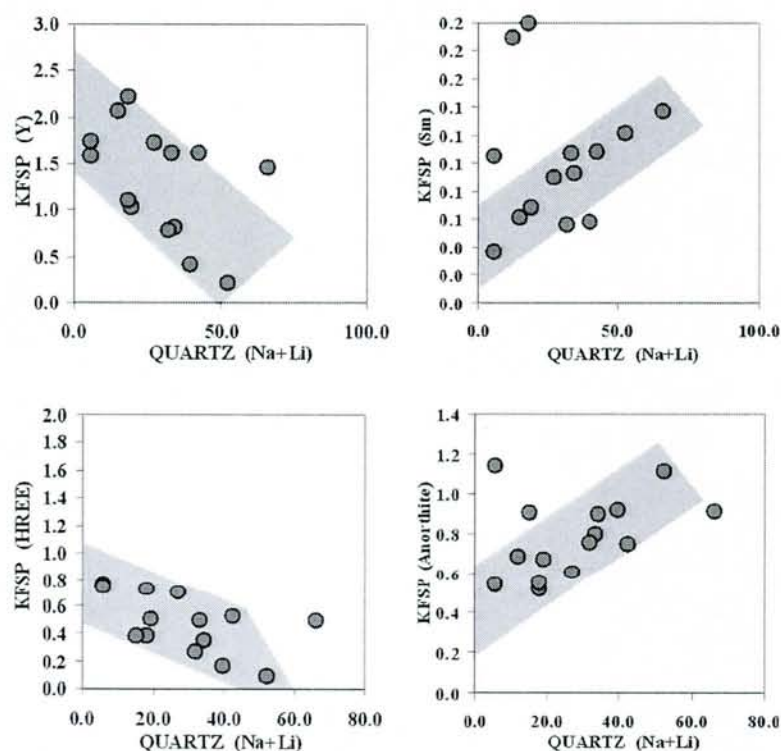


Figure 11: Concentration of charge compensators in core zone and intermediate zone quartz and K-feldspar from both Evje-Iveland and Froland. The concentrations of various elements in K-feldspar are shown on axis to the left whereas the concentration of Na+Li in co-existing quartz is marked on the bottom axis. See text for further explanations

6.3 Exploration strategies

One of the goals of the present project was to define a method that may be used in the exploration after new high-purity quartz occurrences. The results outlined in the previous

sections point to several features that may be very helpful in isolating pegmatite fields which offer a high potential for finding high-purity quartz occurrences. It was shown that the distribution of structural impurities in quartz is highly dependent on the evolution of the co-existing pegmatite forming melts. It is therefore implied that any analytical method that may distinguish between relatively primitive and more evolved granite pegmatites in a given pegmatite field, may be applied in isolating the pegmatites that potentially contain the lowest concentrations of structural impurities in quartz. The method used in the present study was to estimate the trace and major element composition of K-feldspar. K-feldspar is virtually always present in granite pegmatites, is geochemically well known through umpteen studies and the most important major and trace elements are easy to analyse with conventional XRF-methods. The present study imply that simple CaO analysis may suffice in isolating more primitive from more evolved pegmatites because the anorthite concentration is so well correlated with the concentration of Ti, Na and Li in quartz. However, the low concentration of Ca in most pegmatite K-feldspar indicate that Ca should rather be treated as a trace element and be analysed accordingly in order to obtain more precise data. Disregarding the method, Ca is easy to quantify with the XRF method and may, together with the concentration of K, Rb and Sr, be applied in defining the most evolved parts of a pegmatite field. Having this accomplished, the present study implies that feasible quartz deposits are most likely present in the most evolved parts of the pegmatite field. In many pegmatite fields around the world K-feldspar analysis together with other mineralogical studies have established which parts of the pegmatite fields that are most evolved and, therefore, the potentially attractive parts of the pegmatite fields are already delimited.

The next logical step is to continue with LA-HR-ICP-MS analysis of quartz to isolate pegmatites with low concentrations of structural impurities. LA-HR-ICP-MS analysis does not provide the low detection limits as is common with conventional solution ICP-MS analysis, however, the method is rapid and allows the analysis of several hundred samples in a few days. Inherently, LA-HR-ICP-MS analysis are also much cheaper because it is not necessary to go through expensive and time consuming sample preparation procedures, e.g. mineral separation, acid leach and sample digestion that are required before solution ICP-MS of quartz. Finally, when a couple of promising pegmatites are isolated, it may be necessary to apply conventional sample preparation of quartz to evaluate the industrial potential of the deposit. However, if the promising pegmatites are very large and comprise heterogeneous zonation patterns, such as for example the Glamsland pegmatite, isolation of the best parts

may be well accomplished with LA-ablation analysis of quartz, before conventional analysis are applied.

7. CONCLUSIONS

7.1 Industrial application of results

It may be concluded that the analytical procedure that was partially developed in collaboration with Monash University is fully operational and, as it stands, may be applied as an exploration method for identifying new high-purity quartz deposits. The analytical method may also be important in characterising which part of an already existing mining operation that contains the best qualities of quartz. In mapping the quality of quartz throughout an existing mine, it may aid the producer in optimising the potential of the quartz raw material and overall may be an important guide in the day-to-day operation of the quarry.

Compared with conventional methods for analysis of quartz, the analytical method developed at NGU is faster and cheaper, and minimizes the risk of contamination of the sample. The major disadvantage is that the detection limits are rather high compared with conventional methods and that a few important elements (P, Na) cannot presently be analysed. Therefore, the analytical method may primarily be applied to regional exploration and element mapping of existing quartz-operations.

Studies of granite pegmatite quartz in Evje-Iveland and Froland imply that systematic XRF-analysis of selected minerals in granite pegmatites may aid in defining areas where the prospecting after high-purity quartz is most beneficial. In many pegmatite fields, this has already been accomplished so that laser ablation of quartz may proceed right away.

7.2 Structural impurities in quartz

- Studies of the concentration of Al, Be, Mg, K, Ti, Cr, Mn, Fe, Ge, Rb, Sr, Ba, Pb, Th, and U in quartz in the Evje-Iveland and Froland unequivocally demonstrates that granite pegmatite quartz in Froland is more pure than Evje-Iveland quartz.
- The main benefit of the Froland quartz is the low contents of Al, Li, Na. However, the concentration of Ti remains quite high although, on the average, it is lower than Evje-Iveland quartz.
- The trace element distribution in quartz follows the petrogenetic evolution of K-feldspar, which is governed by processes of igneous differentiation in the pegmatite

melts. Accordingly, speciation and quantity of structural admixtures in quartz is also governed by the igneous evolution of the pegmatite forming melt.

- Following the above point, the purity, i.e. the quality of quartz in Evje-Iveland and Froland pegmatite fields is proportional to the degree of differentiation of the pegmatite forming liquids. In other words, the concentration of structural elements incorporated in the quartz crystal structure becomes progressively lower as igneous differentiation proceeds from primitive to more evolved granite pegmatite melts. Future studies may show if this is a general principle that may be applied to pegmatite fields elsewhere in the world.
- In Evje-Iveland, the spatial distribution of the major structural impurities (Al, Li, Na, Ti) decreases towards west and northwest. This trend coincides with the studies of K-feldspar (Larsen *in prep.*) implying that the most primitive pegmatites occur in North and towards East of the Evje-Iveland pegmatite field.

7.3 Analytical strategies

Although the analytical method is applicable as it stands, it would in the long term be desirable to improve the precision of Al and Li analysis. Recent improvements and analysis of well-characterized samples imply that this task is already accomplished.

Analysis of Ca may be possible after the manufacture of better standards and B may be quantified if pre-ablation of the sample surface is applied and if the analyses of $\text{Li}_2\text{B}_4\text{O}_7$ tablets remain discontinued with the LA-HR-ICP-MS instrument at NGU.

The analytical approach used at VIEPS differ from the NGU-method on the following points

- Rather than constructing a calibration curve including several standards, VIEPS applied a two-point calibration curve including NIST612 and the argon blank. This is a common approach used at most laboratories but at low concentrations the calibration-curve may deviate from the trend obtained with a two-point calibration. For most elements, the approach used at NGU gave higher precision.
- At VIEPS, both micro-rastering and spot analysis was acquired whereas only the micro-rastering method was used at NGU. However, at NGU, it was possible to reduce the raster to only $250 \times 250 \mu\text{m}$ and, therefore, the ablated area approached the size produced during common spot analysis. The advantage with raster analysis is that the data-acquisition time is longer hence the precision is improved.

- Many of the interference problems realized during analysis at VIEPS were solved at NGU after that isotope-drift was minimized and LA-analysis in MR and HR-modes could be implemented at a sufficient speed.
- Data processing at VIEPS proceeds considerably more swiftly than at NGU because statistical treatment of the raw-data, including spike removal and identification/removal of outliers, is easily processed with the Schonbein software.

8. RECOMMENDATIONS

- Although the concentration of Ti in quartz in Froland is rather high, this area has fairly low concentrations of Al, Li and Na and, therefore, a more detailed survey should be launched in the Froland area that includes the analysis of both K-feldspar and quartz.
- More analysis of quartz from granite pegmatites in Evje-Iveland and Froland is required in order to consolidate the principle that the trace element distribution in granite pegmatite quartz is a function of igneous differentiation.
- The LA-HR-ICP-MS method must be fine-tuned and has to be developed to include the analysis of B and Ca and if possible P. For many commodities, low concentrations of the transition metals are imperative. Therefore, the final method should also include Cu, Co and Ni. Cu and Co should not pose any problems, however, Ni-contamination from the cones in the mass spectrometer may invalidate analysis of this element at very low concentrations (sub-ppm).

9. Acknowledgement

We are profoundly grateful to North Cape Minerals for generous financial support of the project. Some of the ideas and results presented in this study were conceived during studies and discussions with the staff at Université Paul-Sabatiere, *Laboratoire de Géochimie* and *Laboratoire de Mineralogie et Cristallographie* and at Monash University, VIEPS of RBL. The Leonardo da Vinci programme supported the stay at Université Paul-Sabatiere. Gunnar Juve (NGU) was of profound help at the implementation of this project and in generating some of the necessary funding for studies in France.

10. REFERENCES

- Andersen O (1931). Feldspar II (in Norwegian). *Bulletin Geological Survey of Norway*, **128b**, 1-109.
- Aines, R.D. & Rossman, G.R. 1986: Relationships between radiation damage and trace water in zircon, quartz, and topaz. *American Mineralogist* *71*, 1186-1193.
- Bjørlykke, H. 1935: The mineral paragenesis and classification of the granite pegmatites of Iveland, Setesdal, South Norway. *Norsk Geologisk Tidsskrift* *14*, 211-311.
- Brouard, S., Breton, C. & Giradet, C. 1995: Small alkali metal clusters on (001) quartz surface: adsorption and diffusion. *Journal of Molecular Structure (Theochem)* *334*, 145-153.
- Cerny, P., & Meintzer, R.E., (1988): Fertile granites in the Archean and Proterozoic fields of rare-element pegmatites: crustal environment, geochemistry and petrogenetic relationships. *Canadian Institution Mining and Metallurgy Special Publication* *39*, 170-206.
- Cohen, A.J. & Makar, L.N. 1984: Differing effects of ionizing radiation in massive and single crystal rose quartz. *Neues Jahrbuch für Mineralogie Monatsheft*, 513-521.
- Cohen, A.J., & Makar, L.N. 1985: Dynamic biaxial absorption spectra of Ti^{3+} and Fe^{2+} in a natural rose quartz crystal. *Mineralogical Magazine* *49*, 709-715.
- Deer, W.A., Howie, R.A. & Zussmann, J. (eds.) 1997: *Rock-forming minerals. Orthosilicates. Vol. 1A*, 630 pp.
- Dennen, W.H. 1964: Impurities in quartz. *Geological Society of America Bulletin* *75*, 241-246.
- Dennen, W.H. 1967: Trace elements in quartz as indicators of provenance. *Geological Society of America Bulletin* *78*, 125-130.

- Dennen, W.H., Blackburn, W.H. & Quesada, A. 1970: Aluminium in quartz as a geothermometer. *Contributions to Mineralogy and Petrology* 27, 332-342.
- Falkum, T. 1982: Geological map of Norway, basement map MANDAL – 1:250 000, Geological Survey of Norway.
- Fanderlik, I. (ed.) 1991: *Silica glass and its application*. Elsevier Science Publishing Company, 304 pp.
- Feldmann, I., Tittes, W., Jakubowski, N. & Stuewer, D. (1994) Performance characteristics of inductively coupled plasma mass spectrometry with high mass resolution. *Journal of Analytical Atomic Spectrometry* 9, 1007-1014.
- Fought, H. 1993: *Geological descriptions of pegmatites in the Einerkilen-Ånestølkilen area, South Norway* (in Danish). Unpubl. M.Sc. Thesis, University of Copenhagen, 96 pp + appendix.
- Giebmann, U. & Greb, U. (1994) High resolution ICP-MS – a new concept for elemental spectrometry, *Fresenius Journal of Analytical Chemistry* 350, 186-193.
- Govindaraju, K. (1994). *Geostandard Newsletter*, 18, special issue, p 16 and p 40
- Hassan, F., & Cohen, A.J. 1974: Biaxial color centers in amethyst quartz. *American Mineralogist* 59, 709-718
- Horn, I., Hinton, R.W., Jackson, S.E & Longerich, H.P. (1997) *Geostandard Newsletter*, 21/2, 191-203
- Jung, L. (ed.) 1992: *High-purity natural quartz. Part 1: High-purity natural quartz for industrial use*. Library of Congress-in-Publication Data, New Jersey. 538 pp.
- Lahaye Y., Lambert D. & Walters S. 1997: Ultraviolet laser sampling and high resolution inductively-coupled plasma mass spectrometry

- Larsen, R.B., Polvé, M., Juve, G. & Poitrasson, F. 1998: Composition of volatiles and structural admixtures in quartz in granite pegmatites, Setesdalen, South Norway (*extended abstract*). *Norges geologiske undersøkelse Bulletin* 433, 38-39.
- Larsen, R.B. & Lahaye Y. 1999: Analytical strategies for LA-HR-ICP-MS analysis of quartz. *Geological Survey of Norway Report* 99.127, 22 pp.
- Larsen, R.B., Polvé, M. & Juve, G. 2000: Granite pegmatite quartz from Evje-Iveland: trace element chemistry and implications for the formation of high-purity quartz. *Norges geologiske undersøkelse Bulletin*, *in press*.
- Lehmann, G. & Bambauer, H.U. 1973: Quartzkristalle und ihre Farben. *Angewandte Chemie* 85/7, 281-289.
- Maschmeyer, D. & Lehmann, G. 1983: A trapped-hole center causing rose coloration of natural quartz. *Zeitschrift Kristallografie* 163, 181-196.
- Pearce, N.J., Wiliam, G., Perkins, T., Westgate, J.A., Gorton, M.P., Jackson, S.E, Neal, C.R.& Chenery, S.P. (1997). *Geostandard. Newsletter*, 21/1, 115-144.
- Padget, P. & Maijer, C. (eds.) 1994: The geology of southernmost Norway; an excursion guide. *Norges geologiske undersøkelse Special Publication* 1, 109 pp.
- Paquette, J. & Reeder, R.J. 1995: Relationship between surface structure, growth mechanism, and trace element incorporation in calcite. *Geochimica et Cosmochimica Acta* 59/4, 735.
- Pedersen, S. 1981: Rb/Sr age determinations on the late Proterozoic granitoids from the Evje area, South Norway. *Bulletin of the Geological Society of Denmark* 29, 129-143.
- Perny, B., Eberhardt, P., Ramseyer, K., Mullis, J. & Pankrath, R. 1992: Microdistribution of Al, Li and Na in □ quartz: Possible causes and correlation with short-lived cathodoluminescence. *American Mineralogist* 77, 534-544.

- Shearer, C. K, Papike, J.J. & Jolliff, B. L. (1992): Petrogenetic links among granites and pegmatites in the Harney Peak rare-element granite pegmatite system, Black Hills, South Dakota. *Canadian Mineralogist* 30, 785-809.
- Stockmarr, P. 1994: *A description of pegmatites at Åvesland and Evje , South Norway.* (in Danish); Unpub. M.Sc. thesis, University of Copenhagen, 133 pp + appendix.
- Watt, G.R., Wright, P, Galloway, S. & McLean, C. 1997: Cathodoluminescence and trace element zoning in quartz phenocrysts and xenocrysts. *Geochimica et Cosmochimica Acta* 61/20, 4337-4348.
- Wilcox R.R (1997). Introduction to Robust Estimation and Hypothesis Testing. Academic Press, USA
- Ødegård M., Dundas S.H. Flem B. & Grimstvedt A. 1998: Application of a double-focusing inductively coupled plasma mass spectrometer with laser ablation for the bulk analysis of rare earth elements in rocks fused with $\text{Li}_2\text{B}_4\text{O}_7$. *Fresenius Journal Analytical Chemistry* 362. 477-482.
- Åmli R (1975): Mineralogy and rare earth geochemistry of apatite and xenotime from the Glosarheia granite pegmatite, Froland, southern Norway. *American Mineralogist*, 60, 607-620.
- Åmli R (1977): internal structure and mineralogy of the Glosarheia granite pegmatite, froland, southern Norway. *Bulletin Geological Society of Norway*, 57, 243-262.

11. APPENDIX

Analytical uncertainty derived from sequential analysis of standards

IN PPM	Sample id	median	SD	Relative dev.	Min	Max	# of anal.	Expected concentration	Deviation	Relative deviation
Li	SRM 1830	7.46	5.35	71.6 %	4.08	13.6	3			
	NIST 614	15.7	4.72	30.0 %	9.95	22.9	5	1.74	13.96	802 %
	Nist 616	18.8	9.75	51.9 %	7.12	34.3	11	0.91	17.89	1966 %
	BCS 313	27.4	4.25	15.5 %	22.9	32.3	4			
	BR K1	36.1	12.3	34.2 %	25.8	51.5	4			
	Nist 612	40.9	1.68	4.1 %	37.7	43.1	7	41.54	-0.64	-1.5 %
	RGM-1	71.4	12.6	17.6 %	58.5	88.6	4	57	14.4	25.3 %
	BR FR2	81.8	7.36	9.0 %	72.1	88.7	4			
Be	Nist 616	0.0463	0.134	289.6 %	-0.153	0.348	11	0.0221	0.0242	110 %
	SRM 1830	0.121	0.133	110.6 %	0.0193	0.272	3			
	BR K1	0.155	0.316	204.5 %	-0.312	0.364	4			
	BCS 313	0.255	0.253	99.0 %	0.0144	0.568	4			
	BR FR2	0.321	0.0227	7.1 %	0.288	0.339	4			
	NIST 614	0.671	0.12	17.9 %	0.489	0.785	5	0.76	-0.089	-11.7 %
	RGM-1	2.28	0.207	9.1 %	2	2.5	4	2.4	-0.12	-5.0 %
	Nist 612	37.4	1.33	3.5 %	35	38.8	7	37.73	-0.33	-0.9 %
Mg	BR K1	0.247	1.70	687.2 %	-1.41	2.00	4	30.15	-29.903	-99.2 %
	BCS 313	28.5	39.5	138.5 %	7.99	87.8	4	7.84	20.66	264 %
	Nist 616	35.0	2.26	6.5 %	32.4	39.2	11	35.4	-0.4	-1.1 %
	NIST 614	36.7	3.02	8.2 %	33.1	41.3	5	36.9	-0.2	-0.5 %
	Nist 612	76.8	3.63	4.7 %	70.6	81.3	7	77.44	-0.64	-0.8 %
	BR FR2	186	14.0	7.5 %	168	202	4	78.39	107.61	137 %
	RGM-1	1630	104	6.4 %	1500	1740	4	1689	-59	-3.5 %
	SRM 1830	26300	3060	11.7 %	22800	28400	3	23519	2781	11.8 %
Al	BR K1	166	48.9	29.4 %	102	220	4	26.47	139.53	527 %
	BCS 313	298	189	63.4 %	172	580	4	190	108	56.8 %
	SRM 1830	624	11.2	1.8 %	611	630	3	635.1	-11.1	-1.7 %
	Nist 612	12500	802	6.4 %	11000	13300	7	10582	1918	18.1 %
	BR FR2	12700	2260	17.8 %	9350	14400	4	79.41	12620.59	15893 %
	NIST 614	12900	580	4.5 %	12300	13500	5	10582	2318	21.9 %
	Nist 616	13000	774	5.9 %	12000	13900	11	10582	2418	22.9 %
	RGM-1	83800	6040	7.2 %	74800	87000	4	72508	11292	15.6 %
K	BR K1	-2.78	14.8	-533.6 %	-24.3	9.75	4			
	Nist 616	41.6	10.5	25.1 %	29.3	61.5	11	29	12.6	43.4 %
	BCS 313	64.5	17.0	26.4 %	43.1	79.2	4	41.51	22.99	55.4 %
	Nist 612	72.5	10.1	14.0 %	61.1	88.4	7	66.26	6.24	9.4 %
	NIST 614	105	50.2	47.6 %	61.0	181	5	30	75	250 %
	SRM 1830	294	31.3	10.7 %	259	319	3	332	-38	-11.4 %
	BR FR2	29700	2210	7.4 %	27100	31700	4	28225	1475	5.2 %
	RGM-1	41500	3140	7.6 %	37900	45500	4	35696	5804	16.3 %
Ti	NIST 614	3.07	1.06	34.6 %	1.85	4.69	5	3.2	-0.13	-4.1 %
	Nist 616	4.32	3.46	80.0 %	1.43	12.2	11	2.8	1.52	54.3 %
	BR K1	4.37	3.95	90.4 %	0.0904	8.73	4			
	Nist 612	51.7	6.88	13.3 %	47.3	66.5	7	48.11	3.59	7.5 %
	SRM 1830	58.0	4.83	8.3 %	54.3	63.4	3	65.9	-7.9	-12.0 %
	BCS 313	101	16.1	15.9 %	85.2	121	4	102	-1	-1.0 %

IN PPM	Sample id	median	SD	Relative dev.	Min	Max	# of anal.	Expected concentration	Deviation	Relative deviation
	BR FR2	373	40.6	10.9 %	331	419	4	47.96	325.04	678 %
	RGM-1	1780	51.0	2.9 %	1730	1840	4	1618	162	10.0 %
Cr	BR K1	0.325	0.127	39.0 %	0.149	0.450	4			
	BCS 313	1.21	0.525	43.5 %	0.745	1.78	4			
	NIST 614	1.21	0.225	18.6 %	1.06	1.61	5	0.99	0.22	22.2 %
	RGM-1	2.95	0.598	20.3 %	2.41	3.67	4	3.7	-0.75	-20.3 %
	BR FR2	3.21	0.414	12.9 %	2.65	3.61	4			
	SRM 1830	7.11	0.267	3.8 %	6.80	7.27	3			
	Nist 616	10.9	22.2	204.4 %	0.261	73.9	11	0.24	10.66	4442 %
	Nist 612	39.5	1.25	3.2 %	37.0	40.5	7	39.88	-0.38	-1.0 %
Mn	BR K1	0.258	0.209	81.1 %	0.0115	0.455	4			
	Nist 616	0.561	0.174	30.9 %	0.354	0.958	11	0.58	-0.019	-3.3 %
	NIST 614	1.51	0.116	7.7 %	1.38	1.64	5	1.37	0.14	10.2 %
	BCS 313	1.86	0.400	21.5 %	1.43	2.37	4	1.007	0.853	84.7 %
	BR FR2	6.14	0.371	6.0 %	5.81	6.65	4			
	SRM 1830	10.8	0.256	2.4 %	10.5	11.0	3			
	Nist 612	38.3	0.636	1.7 %	37.0	38.9	7	38.43	-0.13	-0.3 %
	RGM-1	273	16.9	6.2 %	252	291	4	278.8	-5.8	-2.1 %
Fe	BR K1	9.58	4.50	47.0 %	6.46	16.2	4	70	-60.42	-86.3 %
	Nist 616	13.6	2.99	21.9 %	8.41	20.2	11	19	-5.4	-28.4 %
	NIST 614	15.2	1.86	12.3 %	13.3	17.8	5	22.6	-7.4	-32.7 %
	Nist 612	54.0	8.52	15.8 %	49.4	72.9	7	51	3	5.9 %
	BCS 313	104	12.2	11.8 %	85.7	111	4			
	BR FR2	430	67.7	15.7 %	353	493	4			
	SRM 1830	848	2.05	0.2 %	845	850	3	846.3	1.7	0.2 %
	RGM-1	12300	451	3.7 %	11800	12900	4	13010	-710	-5.5 %
Ge	Nist 616	0.257	0.123	47.8 %	0.00577	0.508	11	0.32	-0.063	-19.7 %
	SRM 1830	0.396	0.106	26.9 %	0.333	0.519	3			
	BCS 313	0.418	0.462	110.3 %	-0.144	0.966	4			
	BR FR2	0.515	0.0936	18.2 %	0.421	0.640	4			
	NIST 614	0.993	0.128	12.9 %	0.859	1.19	5	0.95	0.043	4.5 %
	RGM-1	1.08	0.135	12.6 %	0.954	1.26	4			
	BR K1	1.57	0.153	9.7 %	1.48	1.80	4			
	Nist 612	34.6	0.881	2.5 %	33.3	35.8	7	34.64	-0.04	-0.1 %
Rb	BR K1	0.0984	0.125	127.3 %	-0.0762	0.220	4			
	Nist 616	0.101	0.0611	60.2 %	0.0174	0.249	11	0.1	0.001	1.0 %
	BCS 313	0.471	0.185	39.3 %	0.262	0.629	4			
	SRM 1830	0.495	0.101	20.4 %	0.402	0.602	3			
	NIST 614	1.10	0.291	26.4 %	0.805	1.55	5	0.855	0.245	28.7 %
	BR FR2	10.6	1.01	9.5 %	9.92	12.1	4			
	Nist 612	29.8	1.36	4.6 %	27.5	31.7	7	31.4	-1.6	-5.1 %
	RGM-1	154	3.17	2.1 %	151	158	4	150	4	2.7 %
Sr	BR K1	0.225	0.113	50.3 %	0.0671	0.309	4			
	BCS 313	1.68	0.738	44.0 %	1.07	2.69	4			
	BR FR2	6.35	0.586	9.2 %	5.71	6.87	4			
	Nist 616	44.0	2.58	5.9 %	39.7	48.2	11	41.72	2.28	5.5 %
	NIST 614	48.6	1.48	3.1 %	46.6	50.1	5	45.8	2.8	6.1 %
	SRM 1830	48.9	1.02	2.1 %	47.9	49.9	3			
	Nist 612	75.8	2.09	2.8 %	73.8	79.6	7	78.4	-2.6	-3.3 %
	RGM-1	86.0	4.29	5.0 %	81.0	91.0	4	110	-24	-21.8 %

IN PPM	Sample id	median	SD	Relative dev.	Min	Max	# of anal.	Expected concentration	Deviation	Relative deviation
Ba	BR K1	0.233	0.137	58.7 %	0.112	0.418	4			
	Nist 616	3.20	0.491	15.4 %	2.72	4.24	11	2.4	0.8	33.3 %
	NIST 614	3.60	0.323	9.0 %	3.26	4.08	5	3.29	0.31	9.4 %
	BCS 313	7.50	1.09	14.6 %	6.60	8.96	4			
	SRM 1830	11.7	0.508	4.3 %	11.4	12.3	3			
	BR FR2	26.5	0.661	2.5 %	25.8	27.4	4			
	Nist 612	37.5	0.732	2.0 %	36.4	38.3	7	37.74	-0.24	-0.6 %
	RGM-1	696	29.9	4.3 %	666	737	4	810	-114	-14.1 %
Pb	BR K1	0.186	0.0606	32.6 %	0.0999	0.229	4			
	SRM 1830	0.926	0.0643	6.9 %	0.855	0.979	3			
	BCS 313	1.62	2.73	168.1 %	0.186	5.72	4			
	NIST 614	3.45	0.935	27.1 %	2.57	4.62	5	2.32	1.13	48.7 %
	Nist 616	3.60	0.852	23.7 %	2.50	5.59	11	1.85	1.75	94.6 %
	RGM-1	24.4	2.04	8.4 %	21.4	25.9	4	24	0.4	1.7 %
	Nist 612	38.8	3.06	7.9 %	35.8	44.8	7	38.57	0.23	0.6 %
	BR FR2	21700	1630	7.5 %	20300	23400	4	27862.9	-6162.9	-22.1 %
Th	Nist 616	0.0291	0.0225	77.2 %	-0.0164	0.0700	11	0.0252	0.0039	15.5 %
	BR K1	0.0556	0.125	225.3 %	-0.0484	0.235	4			
	BCS 313	0.248	0.353	142.3 %	0.0311	0.773	4			
	SRM 1830	0.269	0.0962	35.8 %	0.198	0.379	3			
	NIST 614	0.864	0.0606	7.0 %	0.808	0.964	5	0.748	0.116	15.5 %
	BR FR2	1.26	0.0816	6.5 %	1.19	1.38	4			
	RGM-1	12.5	1.57	12.5 %	10.4	14.1	4	15	-2.5	-16.7 %
	Nist 612	38.0	2.06	5.4 %	34.0	41.0	7	37.79	0.21	0.6 %
U	Nist 616	0.0900	0.0743	82.5 %	0.0212	0.233	11	0.0721	0.0179	24.8 %
	BR K1	0.417	0.132	31.8 %	0.288	0.582	4			
	BCS 313	0.443	0.363	82.1 %	0.0613	0.936	4			
	SRM 1830	0.460	0.256	55.7 %	0.297	0.756	3			
	BR FR2	0.583	0.0885	15.2 %	0.480	0.665	4			
	NIST 614	0.929	0.149	16.1 %	0.769	1.16	5	0.823	0.106	12.9 %
	RGM-1	6.30	0.402	6.4 %	5.96	6.79	4	5.8	0.5	8.6 %
	Nist 612	36.9	0.787	2.1 %	35.2	37.7	7	37.38	-0.48	-1.3 %